

APPLICATIONS OF A PARTICLE SIMULATION APPROACH

A THESIS SUBMITTED TO
THE GRADUATE SCHOOL OF NATURAL AND APPLIED SCIENCES
OF
MIDDLE EAST TECHNICAL UNIVERSITY

BY

İSMAİL KABAKCI

IN PARTIAL FULFILLMENT OF THE REQUIREMENTS
FOR
THE DEGREE OF MASTER OF SCIENCE
IN
AEROSPACE ENGINEERING

SEPTEMBER 2019

Approval of the thesis:

APPLICATIONS OF A PARTICLE SIMULATION APPROACH

submitted by **İSMAİL KABAKCI** in partial fulfillment of the requirements for the degree of **Master of Science in Aerospace Engineering Department, Middle East Technical University** by,

Prof. Dr. Halil Kalıpçılar
Dean, Graduate School of **Natural and Applied Sciences**

Prof. Dr. İsmail Hakkı Tuncer
Head of Department, **Aerospace Engineering**

Assoc. Prof. Dr. Demirkan Çöker
Supervisor, **Aerospace Engineering, METU**

Prof. Dr. Cahit Çıray
Co-Supervisor, **Aerospace Engineering, METU**

Examining Committee Members:

Prof. Dr. İsmail Hakkı Tuncer
Aerospace Engineering, METU

Assoc. Prof. Dr. Demirkan Çöker
Aerospace Engineering, METU

Prof. Dr. Cahit Çıray
Aerospace Engineering, METU

Prof. Dr. Hasan Umur Akay
Automotive Engineering, Atılım University

Assoc. Prof. Dr. Hande Toffoli
Physics, METU

Date: 12.09.2019

I hereby declare that all information in this document has been obtained and presented in accordance with academic rules and ethical conduct. I also declare that, as required by these rules and conduct, I have fully cited and referenced all material and results that are not original to this work.

Name, Surname: İsmail Kabakcı

Signature:

ABSTRACT

APPLICATIONS OF A PARTICLE SIMULATION APPROACH

Kabakcı, İsmail
Master of Science, Aerospace Engineering
Supervisor: Assoc. Prof. Dr. Demirkan Çöker
Co-Supervisor: Prof. Dr. Cahit Çıray

September 2019, 75 pages

The thesis is intended to utilize a particle simulation approach, introduced for simple particles, for engineering problems in order to study and understand fluid behavior at molecular level.

First, an improvement in force potential estimation is proposed for the original method, which offers notable accuracy increase in simulations in terms of determination of position and momentum trajectories. Afterwards, the improved method is applied to heat diffusion and unidirectional fluid flow simulations.

Within the context of the approach, instantaneous velocities of particles are calculated using simple algebraic equations instead of solving differential equations. Equations are derived from Newton's 2nd Law of Motion and Lennard-Jones Force Potential Theory. For interactions taking place between unlike particles, Lorentz-Berthelot Combination Rule is used.

The method is checked in terms of probability density function of speed distribution, distribution of velocity vector components and pressures at equilibrium state. In the scope of diffusion dynamics, thermal characteristics of particles and volume are tracked in order to perform equilibrium analyses. Furthermore, thermal conductivity

coefficient is calculated. Finally, the variation of density between particles is investigated under unidirectional flow condition.

Simulation results give Maxwell-Boltzmann and Gaussian distribution functions in terms of speed and velocity components respectively. Results on pressure calculation compromise with the classical equation of state. Thermal conductivity coefficient agrees with the experimental data. According to the unidirectional fluid flow simulations, the results imply the tendency of particles to stay closer with increasing unidirectional flow velocity.

Keywords: Molecular Dynamics, Particle Activity, Particle Simulation, Thermal Diffusion, Fluid Flow

ÖZ

BİR PARÇACIK BENZETİM YAKLAŞIMININ UYGULAMALARI

Kabakcı, İsmail
Yüksek Lisans, Havacılık ve Uzay Mühendisliği
Tez Danışmanı: Doç. Dr. Demirkan Çöker
Ortak Tez Danışmanı: Prof. Dr. Cahit Çıray

Eylül 2019, 75 sayfa

Bu tez çalışması, basit parçacıklar için tanımlanmış bir parçacık benzetim yaklaşımından yararlanarak mühendislik problemleri için moleküler seviyede akışkan davranışını inceleme ve anlama gayesini içermektedir.

İlk olarak; mevcut yöntem üzerinde kuvvet potansiyelinin önkestirimine yönelik, benzetimlerde pozisyon ve momentum gidişatlarının belirlenmesi bakımından dikkate değer bir doğruluk artışı sunan bir iyileştirme önerilmiştir. Daha sonrasında, anılan iyileştirilmiş yöntem ısı geçişme ve tek yönlü akışkan akımı benzetimlerine uygulanmıştır.

Bu yaklaşım kapsamında parçacıkların anlık hız değerleri diferansiyel denklem çözümü yerine basit cebirsel denklemler üzerinden hesaplanmaktadır. Denklemler, Newton'un İkinci Hareket Yasası ve Lennard-Jones Kuvvet Potansiyeli Teorisi temel alınarak elde edilmiştir. Farklı akışkan parçacıkları arasındaki etkileşimler için Lorentz-Berthelot Karıştırma Kuralı kullanılmaktadır.

Yöntem; denge durumundaki sürat dağılımının olasılık yoğunluk işlevi, hız vektörü bileşenlerinin dağılımları ve basınçlar bakımından kontrol edilmiştir. Geçişme dinamiği kapsamında denge analizleri için parçacıkların ve hacmin ısı özellikleri

takip edilmiştir. İlave olarak, ısı iletkenlik katsayısı hesaplanmıştır. Son olarak, tek yönlü akış koşulları altında parçacıklar etrafındaki yoğunluğun değişimi incelenmiştir.

Benzetim sonuçları, sürat ve hız vektörü bileşenleri için Maxwell-Boltzmann ve Gaussian dağılım fonksiyonlarını vermektedir. Basınç hesaplama sonuçları, klasik hâl denklemi ile uyum içerisindedir. Isıl iletkenlik katsayısı mevcut deneysel veriler ile örtüşmektedir. Tek yönlü akışkan akımı benzetimlerinin sonuçları, parçacıkların artan tek yönlü akım hızı koşullarında komşu parçacıklara daha yakın olma eğilimine işaret etmektedir.

Anahtar Kelimeler: Molekül Dinamiği, Parçacık Hareketi, Parçacık Benzetimi, Isıl Geçişme, Akışkan Akımı

To my beloved family

ACKNOWLEDGEMENTS

First and foremost, I would like to express my sincere gratitude to my co-supervisor, Prof. Dr. Cahit ıray. It was a great honor and precious experience to have the opportunity to work with him. His visionary ideas inspired me to plumb the depths of the subject and sparked my academic growth. I thankfully appreciate his limitless support, motivation and guidance. Furthermore, I am very grateful to my supervisor, Assoc. Prof. Dr. Demirkan öker for his time and efforts. His motivation helped me to keep my focus on the subject. His professional perspective to handle the subject and his guidance to make research improved my point of view to treat the subject. Moreover, I am also indebted to Őeyma Pınar Eneren Aksoy for her support during my involvement on the subject. Her study shed light on the potential success of the approach subject to this thesis.

I would like to thank the owner of my unconditional love, Cansu, for being in my life. She is not only my wife but also my eternal best friend. I am also looking forward to the meet the newcomer of our family, Ege. I am looking forward to the good times we will be having together and forever.

My two closest friends Tanyel Tekin and Samet Aslan deserve a special thank for this thesis. Tanyel, my second co-supervisor, tracked the progress of my thesis in daily basis and encouraged me to fulfill it successfully. Thank you Samet for making me love Aerospace Engineering Department so much. I would like to send my best wishes to Serap Namlı, Őahin Namlı, GüneŐ Ece Günay, Tuğcan Günay, Rıdvan elebiođlu, Ahmet Yılmaz and Berk Ertürk for their precious friendship making me enjoy the life.

Finally; my parents-in-law, Nilüfer and Nihat, and my sister-in-law, Damla, deserve private thanks because there would be always a missing part in my life if I had not been met them. The most sympathetic person, Berk, I am proud for being my brother. I would like to express my deepest gratitude to my parents Sevgi and Mehmet from who offered me always the best. Mom and dad this work has been dedicated to you...

TABLE OF CONTENTS

ABSTRACT	v
ÖZ	vii
ACKNOWLEDGEMENTS	x
TABLE OF CONTENTS	xi
LIST OF TABLES	xv
LIST OF FIGURES	xvi
LIST OF SYMBOLS	xviii
CHAPTERS	
1. INTRODUCTION	1
1.1. The Motivation	1
1.2. The Purpose of the Work	1
1.3. Review of the Literature	3
1.4. Outline of the Thesis	5
2. THEORY	7
2.1. Introduction	7
2.2. The Fundamental Assumption Related to the Theory	7
2.3. Formulation	7
2.3.1. The Base Equation	8
2.3.2. Utilization of Lennard-Jones Potential	14
2.3.3. Estimation of the Next Potential	15
2.3.4. Relation of Velocity Contributions	17
2.3.5. Time-Step Determination	19

2.3.6. Nondimensionalization.....	20
2.3.7. Determination of Velocity and Position Components	21
2.4. The Equilibrium State, Equilibrium Potential and Velocity Scaling	22
2.5. Effective Zone of Influence, Influence Number and Number of Effective Molecules Factor.....	23
2.6. Interaction Between Unlike Molecules	25
3. IMPLEMENTATION PROCESS OF THE THEORY	27
3.1. Introduction.....	27
3.2. The Flow Chart.....	27
3.3. The Main Code (<i>main.m</i>).....	31
3.3.1. Problem Definition for an Application.....	31
3.3.2. Simulation Parameters.....	31
3.3.3. Initial and Boundary Condition Parameters	32
3.3.4. Performing the Simulation.....	32
3.4. Subroutines.....	32
3.4.1. Definition of Initials Subroutine (<i>define.m</i>)	32
3.4.1.1. Definition of Simulation Variables.....	33
3.4.1.2. Creation of Initial Set Up of Particles and Surrounding Boundaries	33
3.4.2. Boundary Control Subroutines	34
3.4.2.1. Checking Destination Positions of Particles (<i>bCheck.m</i>)	34
3.4.2.2. Elastic Boundary Reflection (<i>bReflection.m</i>).....	35
3.4.2.3. Updates on Position and Velocity Components in Case of a Reflection (<i>bReflection.m</i>).....	36
3.4.2.4. Impacts at Boundaries and Mid-Planes (<i>bReflection.m</i>).....	37

3.4.3. Analysis Subroutines.....	37
3.4.3.1. Thermal Diffusion Analyses (<i>tDiffusion.m</i>).....	38
3.4.3.2. Density Variation Analysis (<i>dVariation.m</i>)	38
3.4.4. Visualization Subroutine (<i>tifVisualization.m</i>)	38
3.4.5. Reporting Subroutine (<i>report.m</i>)	38
4. RESULTS	41
4.1. Introduction	41
4.2. Thermal Diffusion Simulation	41
4.2.1. Investigation of Equilibrium State in Phase-1	42
4.2.1.1. From Energy Perspective	43
4.2.1.2. Associated Speeds and Speed Distributions.....	45
4.2.1.3. Pressures.....	50
4.2.2. Investigation of Equilibrium State and Thermal Diffusion in Phase-2....	52
4.2.2.1. From Energy Perspective	52
4.2.2.2. Associated Speeds and Speed Distributions.....	54
4.2.2.3. Pressures.....	55
4.2.3. Investigation of Thermal Diffusion.....	55
4.2.3.1. Particle Tracking Based Thermal Equilibrium.....	55
4.2.3.2. Fixed Volume Based Thermal Equilibrium	58
4.2.3.3. Calculation of Thermal Conductivity Constant.....	60
4.3. Unidirectional Fluid Flow Simulation	61
4.3.1. Variation of Density of Particles.....	63
4.4. Time-Step Dependence of Simulations	67
4.5. Time Efficiency of Simulations	68

5. CONCLUSIONS	71
REFERENCES	73

LIST OF TABLES

TABLES

Table 2.1. Physical Parameters for Argon	15
Table 2.2. Nondimensionalization Values for Argon	20
Table 4.1. Comparison of the Associated Speeds Results	46
Table 4.2. Pressures at Boundaries (Phase-1)	51
Table 4.3. Pressures at Mid-Planes (Phase-1)	51
Table 4.4. System Pressures (Phase-1)	52
Table 4.5. Comparison of the Associated Speeds Results (Phase-2)	54
Table 4.6. System Pressures (Phase-2)	55
Table 4.7. Comparison of Thermal Conductivity Results with the Literature	61

LIST OF FIGURES

FIGURES

Figure 2.1. Definition Parameters of the L-J Potential for Argon.....	15
Figure 2.2. The Relation of Velocity Contributions	17
Figure 3.1. Flow Chart of the Simulation Process.....	30
Figure 3.2. Jet Colormap Array	33
Figure 3.3. Initial Set Up for Two 1000-Particle Systems.....	34
Figure 3.4. Separated System Boundaries.....	35
Figure 3.5. Velocity and Position Updates for Boundary Crosses at the Corner	36
Figure 3.6. Boundary and Mid-Planes where Impacts are Checked.....	37
Figure 4.1. The System Boundaries During Phase-2.....	42
Figure 4.2. Total Potential Energy in Compartment-1 at 300 Kelvin (Phase-1).....	43
Figure 4.3. Total Potential Energy in Compartment-2 at 120 Kelvin (Phase-1).....	43
Figure 4.4. Velocity Scaling Coefficient in Compartment-1 (Phase-1).....	44
Figure 4.5. Velocity Scaling Coefficient in Compartment-2 (Phase-1).....	45
Figure 4.6. Speed Distribution in Compartment-1 (at 1000 ps, end of Phase-1)	47
Figure 4.7. Speed Distribution in Compartment-2 (at 1000 ps, end of Phase-1)	47
Figure 4.8. Speed Distributions in Compartment-1 at (a)100ps (b)200ps (c)300ps..	48
Figure 4.9. Speed Distributions in Compartment-2 at (a)100ps (b)200ps (c)300ps..	48
Figure 4.10. Profile of Velocity Components in Compartment-1 at the end of Phase-1 along (a)x (b)y (c)z axes	49
Figure 4.11. Profile of Velocity Components in Compartment-2 at the end of Phase-1 along (a)x (b)y (c)z axes	49
Figure 4.12. Profile of Velocity Components along x axis in Compartment-1 at (a)100ps (b)200ps (c)300ps.....	50
Figure 4.13. Profile of Velocity Components along x axis in Compartment-2 at (a)100ps (b)200ps (c)300ps.....	50

Figure 4.14. Total Potential Energy of the System (Phase-2)	53
Figure 4.15. Velocity Scaling Coefficient of the System (Phase-2).....	53
Figure 4.16. Speed Distribution of the System (Phase-2).....	54
Figure 4.17. Velocity Components in Phase-2 along (a)x (b)y (c)z axes	55
Figure 4.18. Initial Positions of Particles for Phase-2	56
Figure 4.19. Positions of Particles after 100 Picoseconds in Phase-2	56
Figure 4.20. Positions of Particles after 200 Picoseconds in Phase-2	57
Figure 4.21. Final Positions of Particles after 2000 Picoseconds in Phase-2.....	57
Figure 4.22. Average Temperature of Initial Particle Groups During Simulation	58
Figure 4.23. Jet Colormap Array to Describe Kinetic Energy of Particles.....	58
Figure 4.24. Initial Positions and Velocities of Particles for Phase-2	59
Figure 4.25. Final Positions and Velocities of Particles for Phase-2.....	59
Figure 4.26. Average Temperature of Initial Compartments During Simulation	60
Figure 4.27. The Structure for Unidirectional Fluid Flow Simulation	62
Figure 4.28. The Initial Setup for Unidirectional Fluid Flow Simulation	63
Figure 4.29. State of Particles at 0.2 Times of the Reference Velocity of Flow	64
Figure 4.30. State of Particles at 0.5 Times of the Reference Velocity of Flow	65
Figure 4.31. State of Particles at the Reference Velocity of Flow	65
Figure 4.32. State of Particles at 2 Times of the Reference Velocity of Flow	66
Figure 4.33. State of Particles at 5 Times of the Reference Velocity of Flow	67
Figure 4.34. Average Velocities for Different Time-Step Selections.....	68
Figure 4.35. Simulation Step Durations for (a)125 (b)1000 (c)8000 Particles	68
Figure 4.36. Dependence of Simulation Step Duration and Number of Particles.....	69
Figure 4.37. Simulation Step Durations for the Thermal Diffusion Simulation	70

LIST OF SYMBOLS

SYMBOLS

	ROMAN SYMBOLS		GREEK SYMBOLS
<i>A</i>	Surface area [m^2]	ΔU	Velocity contribution [m/s]
<i>F</i>	Force [N]	ΔX	Distance along x dir. [m]
<i>I</i>	Influence number [1]	ΔY	Distance along y dir. [m]
<i>M</i>	Molar mass [kg/mol]	ΔZ	Distance along z dir. [m]
<i>N</i>	Number of system particles [1]	Δt	Time-step [s]
<i>NEMF</i>	Number of effective molecules factor [1]	Φ	Potential energy change during the time-step [Nm]
<i>R</i>	Universal gas constant [$J/molK$]	ψ	Force potential energy [Nm]
<i>R_{zone}</i>	Cut-off radius of the effective zone of influence [m]	γ	Interaction constant [1]
<i>T</i>	System temperature [K]	ε	Depth of the potential well [J]
<i>U</i>	Velocity [m/s]	ρ	Density [kg/m^3]
<i>U_{ave}</i>	Average speed [m/s]	σ	Van der Waals radius [m]
<i>U_{mps}</i>	Most probable speed [m/s]		
<i>U_{ref}</i>	Reference speed [m/s]		
<i>U_{rms}</i>	Root-mean-square speed [m/s]		
<i>V</i>	System volume [m^3]		
<i>X</i>	Position in x dir. [m]		
<i>Y</i>	Position in y dir. [m]		
<i>Z</i>	Position in z dir. [m]		
<i>c_t</i>	Motion restriction constant [1]		
<i>i</i>	Particle i [1]		
<i>j</i>	Particle j [1]		
<i>k</i>	Velocity contribution relation constant [1]		
<i>k_b</i>	Boltzmann constant [J/K]		
<i>m</i>	Common particle mass [kg]		
<i>n</i>	Number of moles [mol]		
<i>r</i>	Distance to a reference [m]		
<i>r_{KE}</i>	Velocity scaling factor [1]		
<i>t</i>	Time [s]		
<i>x</i>	Cartesian coordinate x dir. [1]		
<i>y</i>	Cartesian coordinate y dir. [1]		
<i>z</i>	Cartesian coordinate z dir. [1]		

CHAPTER 1

INTRODUCTION

1.1. The Motivation

Although the use of continuum principles helps to understand and forecast the behavior of systems in many engineering and scientific problems successfully, the same thing cannot be spelled out for understanding and the structure of turbulence. The idea of examining turbulence at the microscopic scale is hopefully an attempt in this direction. Therefore, the motivation is to try to describe the particle activity under turbulent flow regime. Within this context, an approach proposed by Çıray [1] inspires to define a formulation and a solution method. Validation of the approach was performed by Eneren [2] and promising results were obtained for the probability density function of the speed distribution, the distribution of velocity components, mean free paths and the pressure. Although the method is designed to solve simple algebraic equations, the number of particles and simulation duration must be very large to investigate turbulent flow regime. Therefore, improvement of the accuracy in calculations is studied in the scope of the thesis in order to reduce cumulative round-off errors. In addition, the approach is implemented to thermal diffusion and unidirectional fluid flow applications to see the applicability of the approach in practice. It is hoped that the continuation in this line will draw information about understanding and structure of turbulence.

1.2. The Purpose of the Work

The purpose of this work is to provide simplified models describing the behavior of some physical phenomena at the molecular level with a high accuracy, which is also important in engineering practice. Molecular Dynamics (MD) enables the prediction of position and momentum trajectories easily for a system of particles, which is very

difficult to observe experimentally. Therefore, MD simulations are utilized for a broad range of applications. There exist various approaches to determine the trajectories of particles, for which some detail is provided in Section 1.3. While conventional approaches are based on the solution of differential equations, a different approach was proposed by Çıray in 2015 [1]. The main idea behind that approach is to model the interactions between particles by solving simple algebraic equations. Since the utilization of MD simulation techniques helps to track historical data of all particles in the approach, it is possible to obtain statistical data similar to literature and make comparisons between these two. Although this approach eliminates truncation errors arising from the solution of differential equations, it still includes round-off errors. Accumulated error surely increases with increasing number of particles and simulation duration. Therefore, it is beneficial to implement improvements to calculation technique in order to decrease accumulating errors. A good way to see the results of improvement in calculation technique is to implement the technique for physical applications.

Thus, the goal of this work is two-fold. The first goal is to improve the available technique in terms of accuracy by taking the motion of particles into consideration for estimating the next potential between interacting particles. The second goal is to apply the improved technique to two scientific applications:

- a. Thermal diffusion phenomenon at the molecular level by investigating
 - the establishment of thermal equilibrium in particle systems,
 - the distributions of speed and velocity vector components and the system pressure at the equilibrium state,
 - the diffusion of thermal energy between particle systems at different initial temperatures.
- b. Behavior of fluid molecules under the effect of a common unidirectional velocity vector (uniform flow) by investigating
 - the variation of density of particles.

1.3. Review of the Literature

MD simulations are commonly utilized in order to model a variety of problems in nature. Study of biomolecules is one of the interesting topics where MD simulations are used frequently for understanding the physical basics of structures and functions of macromolecules. For example; taking the importance of internal motions into consideration by means of MD simulation techniques, the early approach which had assumed proteins as rigid structures was replaced by dynamic models [3]. Furthermore, the self-complementary Deoxyribonucleic Acid (DNA) hexamer 5'd(C-G-T-A-C-G)₂ solution structure was refined with the help of MD simulations [4]. In addition, kinetics of spontaneous micelle formation was examined for different micelle concentrations above the critical concentration [5].

MD simulations are important tools for fluid mechanics studies. For instance, shear viscosities of liquids were calculated using MD simulations [6]. Furthermore, structural and thermodynamic properties, self-diffusion coefficients and reorientation correlation times were modeled for liquid methanol by using different intermolecular potential models [7]. Moreover, formation of eddies was observed in MD simulation of obstructed fluid flow [8].

Other popular areas of MD simulations are solid mechanics and materials science. Related to fracture mechanics studies; the evolution and propagation of cracks and fractures of a sheet of ice, subjected to different stress and compression conditions, were simulated and visualized [9]. Under contact mechanics and tribology topics, the influence of surface roughness for contacting surfaces on friction and adhesion was analyzed by a multiscale MD approach [10]. The effect of chromium on wear behavior of high manganese steel for different wear conditions was evaluated [11]. In nanoimprinting lithography, behavior of copper-nickel alloys was simulated for various proportions of substances [12]. For composite technologies, the stress-strain relations and Young's modulus of elasticity were compared as a result of the carbon-nanotube reinforcement options for Epon 862 composite [13].

A group of interacting particles possess potential energy. Most commonly used models are pairwise potentials. One of the simplest pairwise models is the Lennard-Jones Potential. Lennard-Jones presented a model describing the repulsive and attractive parts of the interaction, the first form of the so-called Lennard-Jones Potential, in order to explain the equation state of a gas using available experimental data [14]. In his model, Buckingham focused on the repulsion zone considering the dominating strong repulsion between atoms at close range because of the interpenetration of complete electron shells [15]. Morse Potential offered a good approximation for the vibrational structure of a diatomic molecule [16].

If the interaction takes place between unlike particles, so called combining rules are utilized in potential formulations. Approximations for the equilibrium distance and the well-depth are suggested for this purpose. Lorentz offered to use the arithmetic average of equilibrium distances which is correct analytically for hard sphere systems [17]. In Berthelot Rule, the well-depth approximation of particles was taken as the geometric average [18]. In addition, Hudson and McCoubrey further developed the well-depth approximation while using the Lorentz approach [19]. Sikora proposed new formulations for the equilibrium distance and the well-depth based on spherically symmetric particles assumption [20]. There exist other approximations such as the two for rare gas systems, proposed by Waldman-Hagler [21] and Tang-Toennies [22]. Moreover, Kong and Chakrabarty formulated another combining rule to be used in Exp 6 Potential formula which was a modified version of Buckingham Potential [23].

In general, MD simulations require the solution of differential equations. There are numerical integration algorithms to make estimations for the solutions. Verlet proposed an algorithm to determine thermo-dynamical properties of Lennard-Jones molecules [24]. Beeman's method was a variant of the Verlet algorithm in a predictor-corrector form [25]. Leapfrog algorithm was evaluated to be superior in representation of energy compared to Verlet and Beeman's algorithms [26]. In a different study, promising less computational needs, Çıray derived a mathematically exact formulation to determine instantaneous velocities by the use of some simplifications

and assumptions [1]. Verification of the aforementioned formulation was performed by Eneren, based on speed distribution, mean free path and pressure results [2].

1.4. Outline of the Thesis

The thesis is divided into five chapters. Chapter 1 is a brief introduction including the motivation, the purpose of the work and review of the literature. Chapter 2 explains the theory and includes physical background information, mathematical derivations and the improvement by estimating the next potential. Chapter 3 introduces and explains the flow chart, the main code and subroutines. Chapter 4 presents and discuss the thermal diffusion and unidirectional fluid flow simulation results and the time efficiency of simulations. Chapter 5 includes a brief conclusion of the study and future work recommendations.

CHAPTER 2

THEORY

2.1. Introduction

This chapter starts by explaining the fundamental assumption related to the theory. Next, the derivation of the formulation to be used in the simulations is presented. Then, some remarks about the construction of the equilibrium state and the control of the total energy of the system are explained. Afterwards, the concept of eliminating the interaction of particles outside an effective zone is introduced and the performance of the concept is illustrated for a symmetrically positioned system. Finally, the potential formula is given in case of an interaction between unlike particles.

2.2. The Fundamental Assumption Related to the Theory

In this study, a set of particles constitutes a system in which each particle is under the effect of other parent particles. Considering the Born-Oppenheimer Approximation, the motion of the nuclei and electrons are separated. Particle interactions are modeled by means of potential models, offering better approximations for simple particles than covalent particles due to the isotropy of pair potentials. Since noble gases are good example of simple particles, Argon is selected to be used in simulations.

2.3. Formulation

In this section, the base equation is derived first. Afterwards, the formula representing the potential between particles is presented. Then, the improvement that considers the dynamics of the particles affecting the potential is introduced. Also, the relation between the velocity contributions due to interaction of particles are formulated in order to obtain same number of equations and unknowns. After determination of time-

step and reference velocity, non-dimensional form of base equation is obtained. Finally, the equations to calculate the velocity and position components are given.

2.3.1. The Base Equation

The base equation is introduced to formulate the motion of particles using Newton's 2nd Law of Motion and Force Potential Theory.

A simple particle (e.g. particle i) of mass m_i is subjected to a force \mathbf{F}_{ij}^* as a result of the interaction with any of the surrounding simple particles (e.g. particle j). Positions of particle i and particle j relative to a fixed origin are denoted by \mathbf{r}_i and \mathbf{r}_j respectively. Total force acting on particle i (\mathbf{F}_i) is the sum of pair interaction forces due to surrounding j particles:

$$\mathbf{F}_i = \sum_{\substack{j=1 \\ (j \neq i)}}^N \mathbf{F}_{ij}^* \quad (2.1)$$

where * symbol is used to denote the interaction between only two particles (the pair interaction) is taken into consideration. Total force acting on particle i can be represented as either position or velocity time derivative of particle i :

$$\mathbf{F}_i = m_i \frac{d^2 \mathbf{r}_i}{dt^2} = m_i \frac{d\mathbf{U}_i}{dt} \quad (2.2)$$

where t is time, and \mathbf{U}_i is the velocity vector of the particle i . Combining Eqn. 2.1 and Eqn. 2.2:

$$m_i \frac{d\mathbf{U}_i}{dt} = \sum_{\substack{j=1 \\ (j \neq i)}}^N \mathbf{F}_{ij}^* \quad (2.3)$$

Now focusing on the interaction between any two particles in the system namely particle i and particle j , all other particles are assumed to be isolated. For this case force, potential, position and velocity terms are denoted by uppercase * symbol. Terms which are not denoted by * symbol are either common particle and simulation

properties or refer to that the interactions of all system particles are taken into consideration. Forces acting on particles due to existence of another can be expressed as the following:

$$\mathbf{F}_i^* = m_i \frac{d^2 \mathbf{r}_i^*}{dt^2} = m_i \frac{d\mathbf{U}_i^*}{dt} \quad (2.4)$$

$$\mathbf{F}_j^* = m_j \frac{d^2 \mathbf{r}_j^*}{dt^2} = m_j \frac{d\mathbf{U}_j^*}{dt} \quad (2.5)$$

Note that these pair forces are the same in magnitude but opposite in direction. Direction of the force acting on particle i is selected as the positive direction of the pair force for convention. Therefore,

$$\mathbf{F}_{ij}^* = \mathbf{F}_i^* = -\mathbf{F}_j^* \quad (2.6)$$

Furthermore, inserting Eqn. 2.4 and Eqn. 2.5 in Eqn. 2.6 and being in compliance with the conservation of momentum:

$$\frac{d\mathbf{U}_i^*}{dt} = -\frac{m_j}{m_i} \frac{d\mathbf{U}_j^*}{dt} \quad (2.7)$$

Also, using combined version of Eqn. 2.4 and Eqn. 2.6 in Eqn. 2.3:

$$\frac{d\mathbf{U}_i}{dt} = \sum_{\substack{j=1 \\ (j \neq i)}}^N \frac{d\mathbf{U}_i^*(j, t)}{dt} \quad (2.8)$$

which shows that the velocity of a particle can be calculated easily if velocity contributions of pair interactions can be determined. Integrating Eqn. 2.8 with respect to time between the starting and ending phases of the one simulation step, namely a simulation time-step (Δt):

$$\mathbf{U}_i(t + \Delta t) - \mathbf{U}_i(t) = \sum_{\substack{j=1 \\ (j \neq i)}}^N [\mathbf{U}_i^*(j, t + \Delta t) - \mathbf{U}_i^*(j, t)] \quad (2.9)$$

$$\mathbf{U}_i(t + \Delta t) = \mathbf{U}_i(t) + \sum_{\substack{j=1 \\ (j \neq i)}}^N \Delta \mathbf{U}_i^*(j, \Delta t) \quad (2.10)$$

where $\Delta \mathbf{U}_i^*(j, \Delta t)$ is the velocity contribution of any surrounding j particle on particle i during simulation time-step. Eqn. 2.10 enables to find resulting velocities of particles in the system at the end of a selected simulation time-step in the form of velocity contribution summations. Writing Eqn. 2.10 for each Cartesian coordinate:

$$U_{x,i}(t + \Delta t) = U_{x,i}(t) + \sum_{\substack{j=1 \\ (j \neq i)}}^N \Delta U_{x,i}^*(j, \Delta t) \quad (2.11)$$

$$U_{y,i}(t + \Delta t) = U_{y,i}(t) + \sum_{\substack{j=1 \\ (j \neq i)}}^N \Delta U_{y,i}^*(j, \Delta t) \quad (2.12)$$

$$U_{z,i}(t + \Delta t) = U_{z,i}(t) + \sum_{\substack{j=1 \\ (j \neq i)}}^N \Delta U_{z,i}^*(j, \Delta t) \quad (2.13)$$

Recalling Eqn. 2.4 and Eqn. 2.6:

$$\mathbf{F}_{ij}^*(r_{ij}^*) = m_i \frac{d\mathbf{U}_i^*}{dr_{ij}^*} \frac{dr_{ij}^*}{dt} \quad (2.14)$$

where \mathbf{r}_{ij} is the relative position vector of particle i with respect to particle j and r_{ij} is the absolute scalar form of \mathbf{r}_{ij} . That is:

$$\mathbf{r}_{ij}^* = X_{ij}^* \mathbf{e}_x + Y_{ij}^* \mathbf{e}_y + Z_{ij}^* \mathbf{e}_z \quad (2.15)$$

$$\begin{aligned} r_{ij}^* &= \sqrt{(X_i^* - X_j^*)^2 + (Y_i^* - Y_j^*)^2 + (Z_i^* - Z_j^*)^2} \\ &= \sqrt{X_{ij}^{*2} + Y_{ij}^{*2} + Z_{ij}^{*2}} \end{aligned} \quad (2.16)$$

Applying the Chain Rule for differentiation:

$$\mathbf{F}_{ij}^*(r_{ij}^*) = m_i \frac{d\mathbf{U}_i^*}{dr_{ij}^*} \left[\frac{dr_{ij}^*}{dX_{ij}^*} \frac{dX_{ij}^*}{dt} + \frac{dr_{ij}^*}{dY_{ij}^*} \frac{dY_{ij}^*}{dt} + \frac{dr_{ij}^*}{dZ_{ij}^*} \frac{dZ_{ij}^*}{dt} \right] \quad (2.17)$$

$$\mathbf{F}_{ij}^*(r_{ij}^*) = m_i \frac{d\mathbf{U}_i^*}{dr_{ij}^*} \left[\frac{X_{ij}^*}{r_{ij}^*} U_{x,ij}^* + \frac{Y_{ij}^*}{r_{ij}^*} U_{y,ij}^* + \frac{Z_{ij}^*}{r_{ij}^*} U_{z,ij}^* \right] \quad (2.18)$$

Terms in brackets can also be written in a vector form:

$$\mathbf{F}_{ij}^*(r_{ij}^*) = m_i \frac{\mathbf{r}_{ij}^*(\mathbf{U}_i^* - \mathbf{U}_j^*)}{r_{ij}^*} \frac{d\mathbf{U}_i^*}{dr_{ij}^*} \quad (2.19)$$

Recalling Eqn. 2.7:

$$\frac{d\mathbf{U}_i^*}{dr_{ij}^*} \frac{dr_{ij}^*}{dt} = -\frac{m_j}{m_i} \frac{d\mathbf{U}_j^*}{dr_{ij}^*} \frac{dr_{ij}^*}{dt} \quad (2.20)$$

$$\frac{d\mathbf{U}_i^*}{dr_{ij}^*} = -\frac{m_j}{m_i} \frac{d\mathbf{U}_j^*}{dr_{ij}^*} \quad (2.21)$$

Then Eqn. 2.17 takes the following form:

$$\mathbf{F}_{ij}^*(r_{ij}^*) = m_i \frac{\mathbf{r}_{ij}^*}{r_{ij}^*} \left[\frac{d}{dr_{ij}^*} \left(\frac{U_i^{*2}}{2} \right) + \frac{m_j}{m_i} \frac{d}{dr_{ij}^*} \left(\frac{U_j^{*2}}{2} \right) \right] \quad (2.22)$$

Note that pair force is in the direction of the line connecting the centers of the particles in Eqn. 2.22 as expected due to Newton's 2nd Law of motion.

Considering the force potential theory, the pair force on particle i under the effect of particle j is described by the following equation:

$$\mathbf{F}_{ij}^*(r_{ij}^*) = -\nabla_{\mathbf{r}_i^*} \psi_{ij}(r_{ij}^*) \quad (2.23)$$

$$\mathbf{F}_{ij}^*(r_{ij}^*) = -\left(\frac{\partial}{\partial X_i^*} \mathbf{e}_x + \frac{\partial}{\partial Y_i^*} \mathbf{e}_y + \frac{\partial}{\partial Z_i^*} \mathbf{e}_z \right) \psi_{ij}(r_{ij}^*) \quad (2.24)$$

$$\mathbf{F}_{ij}^*(r_{ij}^*) = -\left(\frac{\partial r_{ij}^*}{\partial X_i^*} \mathbf{e}_x + \frac{\partial r_{ij}^*}{\partial Y_i^*} \mathbf{e}_y + \frac{\partial r_{ij}^*}{\partial Z_i^*} \mathbf{e}_z \right) \frac{d\psi_{ij}(r_{ij}^*)}{dr_{ij}^*} \quad (2.25)$$

$$\mathbf{F}_{ij}^*(r_{ij}^*) = -\left(\frac{X_{ij}^*}{r_{ij}^*} \mathbf{e}_x + \frac{Y_{ij}^*}{r_{ij}^*} \mathbf{e}_y + \frac{Z_{ij}^*}{r_{ij}^*} \mathbf{e}_z \right) \frac{d\psi_{ij}(r_{ij}^*)}{dr_{ij}^*} \quad (2.26)$$

$$\mathbf{F}_{ij}^*(r_{ij}^*) = -\frac{\mathbf{r}_{ij}^*}{r_{ij}^*} \frac{d\psi_{ij}^*}{dr_{ij}^*} \quad (2.27)$$

where ψ_{ij} term represents the force potential between i and j particles. Note that Eqn. 2.22 and Eqn. 2.27 describe the same pair force from two different perspectives and they are equal. Therefore, these two equations can be combined as:

$$m_i \frac{\mathbf{r}_{ij}^*}{r_{ij}^*} \left[\frac{d}{dr_{ij}^*} \left(\frac{U_i^{*2}}{2} \right) + \frac{m_j}{m_i} \frac{d}{dr_{ij}^*} \left(\frac{U_j^{*2}}{2} \right) \right] + \frac{\mathbf{r}_{ij}^*}{r_{ij}^*} \frac{d\psi_{ij}^*}{dr_{ij}^*} = 0 \quad (2.28)$$

$$\frac{1}{2} \left[m_i \frac{dU_i^{*2}}{dr_{ij}^*} + m_j \frac{dU_j^{*2}}{dr_{ij}^*} \right] + \frac{d\psi_{ij}^*}{dr_{ij}^*} = 0 \quad (2.29)$$

which shows that the sum of kinetic and potential energy terms is constant and the total energy is conserved in calculations. Rearranging and integrating Eqn. 2.29 during a simulation time-step:

$$\left[U_i^{*2}(j, t + \Delta t) - U_i^{*2}(t) + \frac{m_j}{m_i} [U_j^{*2}(i, t + \Delta t) - U_j^{*2}(t)] \right] + \frac{2}{m_i} [\psi_{ij}^*(t + \Delta t) - \psi_{ij}^*(t)] = 0 \quad (2.30)$$

$$\psi_{ij}^*(t + \Delta t) - \psi_{ij}^*(t) = \Phi_{ij}^*(\Delta t) \quad (2.31)$$

It is important to note that in Eqn. 2.30, the velocity terms of particle i and particle j at the end of time-step imply the velocity of particles under the effect of each other only. The term given in Eqn. 2.31, which also appears in Eqn. 2.30, represents the potential change during the time-step. Only the interaction between two particles should be taken into consideration for this change. Since the motion of the particles is highly restricted as detailed in Section 2.3.5, the effect of previous particle velocities can be neglected in order to estimate the next force potential between the particles.

Velocities and squares of speeds, given in Eqn. 2.30, at the end of the time-step can be written as:

$$\mathbf{U}_i^*(j, t + \Delta t) = \mathbf{U}_i^*(t) + \Delta \mathbf{U}_i^*(j, \Delta t) \quad (2.32)$$

$$\Delta \mathbf{U}_i^*(j, \Delta t) = \Delta U_{x,i}^*(j, \Delta t) \mathbf{e}_x + \Delta U_{y,i}^*(j, \Delta t) \mathbf{e}_y + \Delta U_{z,i}^*(j, \Delta t) \mathbf{e}_z \quad (2.33)$$

$$U_i^{*2}(j, t + \Delta t) = U_{x,i}^{*2}(j, t + \Delta t) + U_{y,i}^{*2}(j, t + \Delta t) + U_{z,i}^{*2}(j, t + \Delta t) \quad (2.34)$$

$$U_{x,i}^{*2}(j, t + \Delta t) = U_{x,i}^{*2}(t) + 2U_{x,i}^*(t)\Delta U_{x,i}^*(j, \Delta t) + \Delta U_{x,i}^{*2}(j, \Delta t) \quad (2.35)$$

Note that, four equations above are also applicable for surrounding j particles. Furthermore, Eqn. 2.35 can be expressed in y and z directions similarly. Due to conservation of momentum, following relation is valid for all pair interactions:

$$\Delta \mathbf{U}_j^*(i, \Delta t) = -\frac{m_i}{m_j} \Delta \mathbf{U}_i^*(j, \Delta t) \quad (2.36)$$

Applying the relations in Eqn. 2.31, Eqn. 2.34, Eqn. 2.35 and Eqn. 2.36 to Eqn. 2.30:

$$\begin{aligned} & \Delta U_i^{*2}(j, \Delta t) + 2\mathbf{U}_i^*(t)\Delta \mathbf{U}_i^*(j, \Delta t) \\ & + \frac{m_j}{m_i} \left[\left(\frac{m_i}{m_j} \right)^2 \Delta U_i^{*2}(j, \Delta t) \right. \\ & \left. - 2 \left(\frac{m_i}{m_j} \right) \mathbf{U}_j^*(t)\Delta \mathbf{U}_i^*(j, \Delta t) \right] + \frac{2}{m_i} \Phi_{ij}^*(\Delta t) = 0 \end{aligned} \quad (2.37)$$

$$\begin{aligned} & \left(1 + \frac{m_i}{m_j} \right) \Delta U_i^{*2}(j, \Delta t) + 2[\mathbf{U}_i^*(t) - \mathbf{U}_j^*(t)]\Delta \mathbf{U}_i^*(j, \Delta t) \\ & + \frac{2}{m_i} \Phi_{ij}^*(\Delta t) = 0 \end{aligned} \quad (2.38)$$

Using Eqn. 2.33 in Eqn. 2.38:

$$\begin{aligned} & \left(1 + \frac{m_i}{m_j} \right) [\Delta U_{x,i}^{*2}(j, \Delta t) + \Delta U_{y,i}^{*2}(j, \Delta t) + \Delta U_{z,i}^{*2}(j, \Delta t)] \\ & + 2 \left[(U_{x,i}^*(t) - U_{x,j}^*(t)) \Delta U_{x,i}^*(j, \Delta t) \right. \\ & + (U_{y,i}^*(t) - U_{y,j}^*(t)) \Delta U_{y,i}^*(j, \Delta t) \\ & \left. + (U_{z,i}^*(t) - U_{z,j}^*(t)) \Delta U_{z,i}^*(j, \Delta t) \right] + \frac{2}{m_i} \Phi_{ij}^*(\Delta t) \\ & = 0 \end{aligned} \quad (2.39)$$

2.3.2. Utilization of Lennard-Jones Potential

Starting from Eqn. 2.23, the formulation contains a term representing the potential energy between interacting particles. There are number of models to represent this potential in the literature as detailed in Section 1.3. For this study, the Lennard-Jones Potential (also referred to as L-J Potential or 12-6 Potential) is utilized to the formulation considering its ease of implementation and computational efficiency. The potential is defined as a function of distance between particles. More complex force potential models exist offering better accuracy but bringing along more simulation time need.

The L-J Potential for two interacting particles, namely particle i and particle j , is defined as:

$$\psi_{ij}(r_{ij}) = 4\varepsilon \left[\left(\frac{\sigma}{r_{ij}} \right)^{12} - \left(\frac{\sigma}{r_{ij}} \right)^6 \right] \quad (2.40)$$

where ε is the well-depth which is a measure of attraction strength and σ is the the distance at which the intermolecular potential between the particles is zero and also referred to as Van der Waals radius. σ also defines the touch distance between the centers for nonionic particles and it is taken as the half of the internuclear distance between them [14]. The first term (12th power) of the L-J potential equation models the repulsion while the latter term (6th power) describes the attraction between particles. The minimum potential is obtained at $r_{ij} = \sqrt[6]{2}\sigma = 1.1225\sigma$, as illustrated in Figure 2.1. Referencing the equilibrium distance between the centers; as the distance between particles increases, attractive force is observed and the potential tends to zero if r_{ij} tends to infinity. Referencing the equilibrium distance between the centers again; decreasing distance between particles yields a repulsive force which gets stronger and the potential tends to zero if r_{ij} is equal to the equilibrium distance. The equation is also defined for values smaller than the equilibrium distance which indicates that great repulsive force is observed in case a particle is in projection of locating the fictitious shell of another particle.

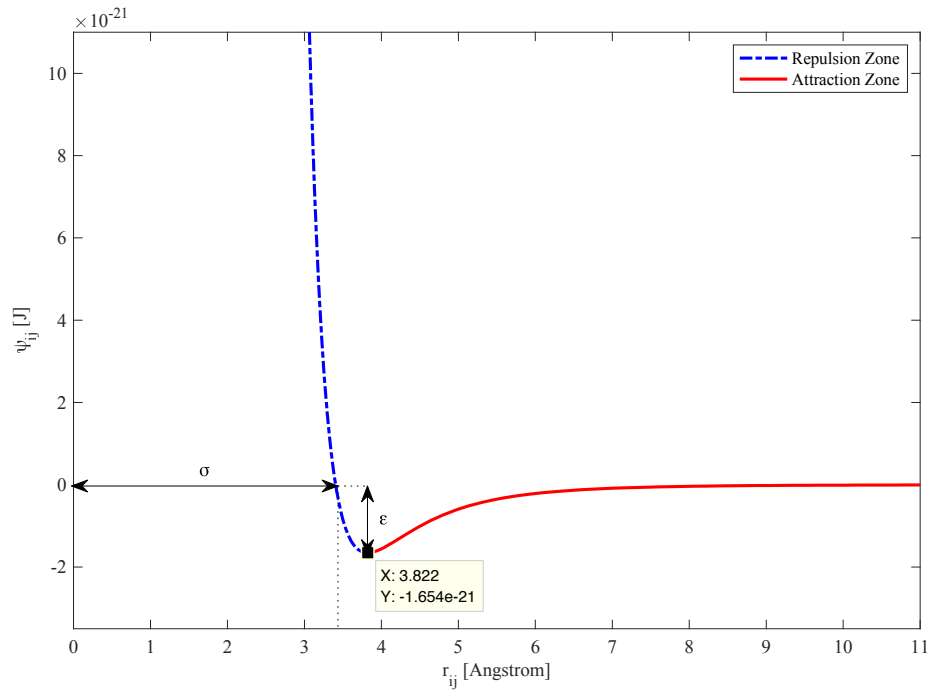


Figure 2.1. Definition Parameters of the L-J Potential for Argon

Physical parameters in the literature [27], presented in Table 2.1, are used in order to perform simulation for Argon particles.

Table 2.1. Physical Parameters for Argon

Parameter	Value	Unit
σ	3.405	[\AA]
ϵ/k_b	119.8	[K]
k_b	$1.380648 \cdot 10^{-23}$	[J/K]

2.3.3. Estimation of the Next Potential

After integration of Eqn. 2.29, the method needs the potential difference to be determined as result of interaction force, which the particle pair is subjected during

time-step, presented in Eqn. 2.31. Expanding the force term given in Eqn. 2.27 for particle i , following equation is obtained:

$$m_i \frac{d^2 \mathbf{r}_i^*}{dt^2} = - \frac{\mathbf{r}_{ij}^* d\psi_{ij}^*}{r_{ij}^* dr_{ij}^*} \quad (2.41)$$

The latter term can be found by taking derivative of Eqn. 2.40:

$$m_i \frac{d^2 \mathbf{r}_i^*}{dt^2} = - \frac{\mathbf{r}_{ij}^*}{r_{ij}^*} \left\{ - \frac{24\varepsilon}{r_{ij}^*} \left[2 \left(\frac{\sigma}{r_{ij}^*} \right)^{12} - \left(\frac{\sigma}{r_{ij}^*} \right)^6 \right] \right\} \quad (2.42)$$

After making rearrangements, the acceleration of particle i can be calculated as:

$$\frac{d^2 \mathbf{r}_i^*}{dt^2} = \frac{\mathbf{r}_{ij}^*}{r_{ij}^*} \left\{ \frac{24\varepsilon}{m_i r_{ij}^*} \left[2 \left(\frac{\sigma}{r_{ij}^*} \right)^{12} - \left(\frac{\sigma}{r_{ij}^*} \right)^6 \right] \right\} \quad (2.43)$$

In order to determine the potential after the interaction, the distance between particles after the interaction should be estimated. Assuming that the acceleration given in Eqn. 2.43 is constant during the simulation, the distance can be simply obtained from position-acceleration relations:

$$\mathbf{r}_{ij}^*(t + \Delta t) = \mathbf{r}_{ij}^*(t) + \frac{1}{2} \frac{d^2 \mathbf{r}_{ij}^*(j, \Delta t)}{dt^2} \Delta t^2 \quad (2.44)$$

Eqn. 2.43 gives the acceleration of particle i . If particles in the system are identical, i.e. particle i and particle j are the same particles, the relative acceleration between particles is two times of the acceleration of particle i . Otherwise, particle accelerations will be inversely proportional with respect to their masses. Inserting the acceleration term in Eqn. 2.43 into Eqn. 2.44:

$$\begin{aligned} \mathbf{r}_{ij}^*(t + \Delta t) = & \mathbf{r}_{ij}^*(t) \\ & + \left\{ \left(\frac{m_i + m_j}{m_i m_j} \right) \frac{12\varepsilon}{r_{ij}^{*2}(t)} \left[2 \left(\frac{\sigma}{r_{ij}^*(t)} \right)^{12} \right. \right. \\ & \left. \left. - \left(\frac{\sigma}{r_{ij}^*(t)} \right)^6 \right] \mathbf{r}_{ij}^*(t) \right\} \Delta t^2 \end{aligned} \quad (2.45)$$

Calculating the magnitude of the next distance $r_{ij}^*(t + \Delta t)$, the potential after the interaction can be estimated as:

$$\psi_{ij}(t + \Delta t) = 4\varepsilon \left[\left(\frac{\sigma}{r_{ij}^*(t + \Delta t)} \right)^{12} - \left(\frac{\sigma}{r_{ij}^*(t + \Delta t)} \right)^6 \right] \quad (2.46)$$

2.3.4. Relation of Velocity Contributions

Eqn. 2.39 is insufficient to describe the interaction itself because there are still unknown velocity contributions in each direction. As found in Eqn. 2.43 and being compatible with Newton's 2nd Law of Motion; the acceleration vector, arising due to the interaction, is along the line connecting particle centers. Therefore; the force and the velocity contribution should also be along the same line which implies the relation of velocity contributions in each direction, as Figure 2.2 describes an attraction case in two dimensions.

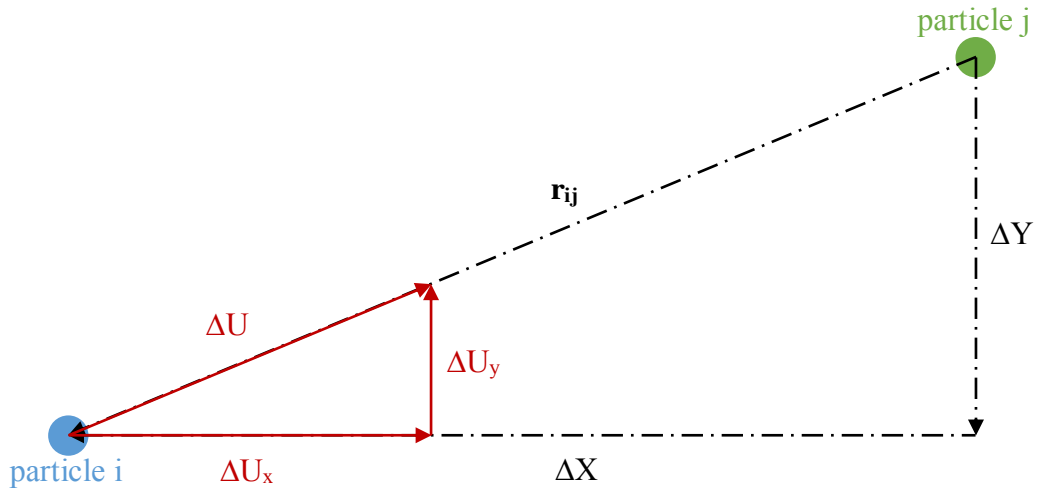


Figure 2.2. The Relation of Velocity Contributions

Note that velocity contribution vector is a unit vector, just describing the direction. The velocity contribution is the multiplication of the average acceleration and the time-step:

$$\Delta U_i^*(j, \Delta t) = \frac{\overline{d^2 r_i^*(j, \Delta t)}}{dt^2} \Delta t \quad (2.47)$$

where $\Delta U_i^*(j, \Delta t)$ term is used to describe the velocity contribution for particle i due to the interaction with particle j during the time-step Δt . To determine average accelerations, the acceleration of particle i can be calculated using the distance between the particles for the start and finish set up:

$$\frac{\overline{d^2 X_i^*(j, \Delta t)}}{dt^2} = \frac{1}{2} \left[\frac{d^2 X_i^*(j, t + \Delta t)}{dt^2} + \frac{d^2 X_i^*(j, t)}{dt^2} \right] \quad (2.48)$$

$$\frac{\Delta U_{x,i}^*(j, \Delta t)}{\Delta U_{y,i}^*(j, \Delta t)} = \frac{\frac{\overline{d^2 X_i^*(j, \Delta t)}}{dt^2}}{\frac{\overline{d^2 Y_i^*(j, \Delta t)}}{dt^2}} = \frac{\frac{d^2 X_i^*(j, t + \Delta t)}{dt^2} + \frac{d^2 X_i^*(j, t)}{dt^2}}{\frac{d^2 Y_i^*(j, t + \Delta t)}{dt^2} + \frac{d^2 Y_i^*(j, t)}{dt^2}} \quad (2.49)$$

$$\begin{aligned} \frac{\Delta U_{x,i}^*(j, \Delta t)}{\Delta U_{y,i}^*(j, \Delta t)} &= \frac{\frac{\Delta X(t + \Delta t)}{r_{ij}(t + \Delta t)} + \frac{\Delta X(t)}{r_{ij}(t)}}{\frac{\Delta Y(t + \Delta t)}{r_{ij}(t + \Delta t)} + \frac{\Delta Y(t)}{r_{ij}(t)}} \\ &= \frac{\Delta X(t + \Delta t) r_{ij}(t) + \Delta X(t) r_{ij}(t + \Delta t)}{\Delta Y(t + \Delta t) r_{ij}(t) + \Delta Y(t) r_{ij}(t + \Delta t)} = \frac{k_x}{k_y} \end{aligned} \quad (2.50)$$

where k_x and k_y parameters are used to simplify the relations. Next positions are estimated using Eqn. 2.45. The remedy is also applicable in z-direction and following relation can be written:

$$k = \sqrt{k_x^2 + k_y^2 + k_z^2} \quad (2.51)$$

Using these relations, Eqn. 2.39 can be reduced to one unknown:

$$\begin{aligned}
& \left(1 + \frac{m_i}{m_j}\right) \left[\frac{k_x^2 + k_y^2 + k_z^2}{k_x^2} \right] \Delta U_{x,i}^{*2}(j, \Delta t) \\
& + 2 \left[\left(U_{x,i}^*(t) - U_{x,j}^*(t) \right) \right. \\
& + \left(U_{y,i}^*(t) - U_{y,j}^*(t) \right) \frac{k_y}{k_x} \\
& + \left. \left(U_{z,i}^*(t) - U_{z,j}^*(t) \right) \frac{k_z}{k_x} \right] \Delta U_{x,i}^*(j, \Delta t) \\
& + \frac{2}{m_i} \Phi_{ij}^*(\Delta t) = 0
\end{aligned} \tag{2.52}$$

$$\begin{aligned}
& \left(1 + \frac{m_i}{m_j}\right) \frac{k^2}{k_x} \Delta U_{x,i}^{*2}(j, \Delta t) \\
& + 2 \left[\left(U_{x,i}^*(t) - U_{x,j}^*(t) \right) k_x \right. \\
& + \left(U_{y,i}^*(t) - U_{y,j}^*(t) \right) k_y \\
& + \left. \left(U_{z,i}^*(t) - U_{z,j}^*(t) \right) k_z \right] \Delta U_{x,i}^*(j, \Delta t) \\
& + \frac{2k_x}{m_i} \Phi_{ij}^*(\Delta t) = 0
\end{aligned} \tag{2.53}$$

2.3.5. Time-Step Determination

The most important effect of the time-step (Δt) choice is to limit the motion of particles during a simulation step time interval. The motion of the particles should be restricted not only to prevent a particle to pass over another but also to ensure the validity and stability of the formulation. However, increase in number of simulation steps leads to inefficiency in terms of CPU time. Two particles separated by 1.1225 times of the diameter, are in equilibrium state with no interaction force. However, if the particles come closer by 0.1225 times of the diameter, collision happens. Therefore, particles are restricted to move 5% of their diameter at a reference velocity in this study. More details about the reference velocity and time-step are provided in Section 2.3.6. Time-step dependence and time efficiency of simulations are further analyzed with examples in Section 4.4 and Section 4.5.

2.3.6. Nondimensionalization

In many engineering problems, non-dimensional units are defined to simplify the equations and to improve the precision. Hence, parameters are nondimensionalized according to the reference data given in *Table 2.2*.

Table 2.2. *Nondimensionalization Values for Argon*

Parameter	Reference Dimension	Value	Unit
Position	σ	3.405	[\AA]
Velocity	$U_{ref} = \sqrt{\frac{8\varepsilon}{m}}$	446.7	[m/s]
Time	$\frac{c_t \sigma}{U_{ref}}$	0.038	[ps]

Here, c_t and U_{ref} are defined as the motion restriction constant and the reference speed respectively. By nondimensionalization of Eqn. 2.53:

$$\begin{aligned}
 & \left(1 + \frac{m_i}{m_j}\right) \frac{k^2}{k_x} \Delta U_{x,i}^{*2}(j, \Delta t) \\
 & + 2 \left[\left(U_{x,i}^*(t) - U_{x,j}^*(t) \right) k_x \right. \\
 & + \left(U_{y,i}^*(t) - U_{y,j}^*(t) \right) k_y \\
 & + \left. \left(U_{z,i}^*(t) - U_{z,j}^*(t) \right) k_z \right] \Delta U_{x,i}^*(j, \Delta t) \\
 & + k_x \Phi_{ij}^*(\Delta t) = 0
 \end{aligned} \tag{2.54}$$

Non-dimensional form of Eqn. 2.40 and Eqn. 2.45:

$$\psi_{ij}(r_{ij}) = [r_{ij}^{-12} - r_{ij}^{-6}] \tag{2.55}$$

$$\begin{aligned}
 \mathbf{r}_{ij}^*(t + \Delta t) = & \mathbf{r}_{ij}^*(t) \\
 & + \left\{ 3 \left(\frac{m_i + m_j}{m_j} \right) [2r_{ij}^{*-14}(t) \right. \\
 & \left. - r_{ij}^{*-8}(t)] \mathbf{r}_{ij}^*(t) \right\} \Delta t^2
 \end{aligned} \tag{2.56}$$

2.3.7. Determination of Velocity and Position Components

Solving the 2nd order equation in Eqn. 2.54 and making the following simplification, which is given in Eqn. 2.57:

$$part = U_{x,ij}^*(t)k_x + U_{y,ij}^*(t)k_y + U_{z,ij}^*(t)k_z \quad (2.57)$$

$$\Delta U_{x,i}^*(j, \Delta t) = \left[-part \pm \sqrt{part^2 - \frac{m_i + m_j}{m_i m_j} k^2 \Phi_{ij}^*(\Delta t)} \right] \frac{m_j k_x}{(m_i + m_j)k^2} \quad (2.58)$$

$$\Delta U_{x,i}^*(j, \Delta t) = \left[-part + \gamma \sqrt{part^2 - \frac{m_i + m_j}{m_i m_j} k^2 \Phi_{ij}^*(\Delta t)} \right] \frac{m_j k_x}{(m_i + m_j)k^2} \quad (2.59)$$

As discussed in Section 2.3.4, only the interaction force effect is taken into consideration for potential difference calculation. Since the motion of the particle is very limited during a time-step of the simulation, it is possible to simplify Eqn. 2.59:

$$\Delta U_{x,i}^*(j, \Delta t) = \frac{\gamma m_j k_x}{(m_i + m_j)k^2} \sqrt{-\frac{m_i + m_j}{m_i m_j} k^2 \Phi_{ij}^*(\Delta t)} \quad (2.60)$$

The idea is to freeze all particles at the beginning of a time-step, allowing them to interact with other particles while neglecting the velocities, they have. This results the *part* term to be zero. After calculating new velocities and positions, effect of these velocities is added. This idea brings the Eqn. 2.59 to the form of Eqn. 2.60, where γ term to only take -1 or 1 value for attraction or repulsion occurrence of interaction respectively. Velocity contributions in other coordinates can be found as similar:

$$\Delta U_{y,i}^*(j, \Delta t) = \frac{\gamma m_j k_y}{(m_i + m_j)k^2} \sqrt{-\frac{m_i + m_j}{m_i m_j} k^2 \Phi_{ij}^*(\Delta t)} \quad (2.61)$$

$$\Delta U_{z,i}^*(j, \Delta t) = \frac{\gamma m_j k_z}{(m_i + m_j) k^2} \sqrt{-\frac{m_i + m_j}{m_i m_j} k^2 \Phi_{ij}^*(\Delta t)} \quad (2.62)$$

New velocity vector components can be calculated using the velocity contributions by the expansion of Eqn. 2.10:

$$U_{x,i}(t + \Delta t) = U_{x,i}(t) + \sum_{\substack{j=1 \\ (j \neq i)}}^N \Delta U_{x,i}^*(j, \Delta t) \quad (2.63)$$

$$U_{y,i}(t + \Delta t) = U_{y,i}(t) + \sum_{\substack{j=1 \\ (j \neq i)}}^N \Delta U_{y,i}^*(j, \Delta t) \quad (2.64)$$

$$U_{z,i}(t + \Delta t) = U_{z,i}(t) + \sum_{\substack{j=1 \\ (j \neq i)}}^N \Delta U_{z,i}^*(j, \Delta t) \quad (2.65)$$

Since the previous positions and velocities of particles are known and the velocity interactions are determined, new positions of the particles can be calculated:

$$X_i(t + \Delta t) = X_i(t) + U_{x,i}(t + \Delta t) \Delta t \quad (2.66)$$

$$Y_i(t + \Delta t) = Y_i(t) + U_{y,i}(t + \Delta t) \Delta t \quad (2.67)$$

$$Z_i(t + \Delta t) = Z_i(t) + U_{z,i}(t + \Delta t) \Delta t \quad (2.68)$$

2.4. The Equilibrium State, Equilibrium Potential and Velocity Scaling

Initially, the particles in the system are located in any desired configuration and given the same speed according to the system temperature. Furthermore, the velocity vector directions are determined randomly. Therefore, initial system configuration is not in equilibrium state. Two indicators can be defined to control whether the system reached the equilibrium state or not.

Although it is also easy to model otherwise, it is assumed that the system is isolated. Hence, the total energy of the particles should be conserved in all simulation steps. As

a first indicator of equilibrium state, the total potential energy of the system should converge to zero. For each simulation step, total potential energy of the system is calculated using Eqn. 2.69:

$$\psi_{system}(t) = \sum_{i=1}^N \sum_{\substack{j=1 \\ (j>i)}}^N \psi_{ij}^*(t) \quad (2.69)$$

Another indicator for equilibrium is the square root of the ratio of the initial total kinetic energy of the system to the instantaneous total kinetic energy in the simulation step, i.e. r_{KE} , given in Eqn. 2.70. In equilibrium state, r_{KE} should converge to 1.

$$r_{KE}(t + \Delta t) = \sqrt{\frac{Q(t = 0)}{Q(t + \Delta t)}} = \sqrt{\frac{\sum_{i=1}^N U_i^2(t = 0)}{\sum_{i=1}^N U_i^2(t + \Delta t)}} \quad (2.70)$$

Total kinetic energy, i.e. Q , is calculated in each simulation step. Since the system is isolated, all calculated velocities are multiplied by the corresponding r_{KE} before calculating the final positions. This method is called as velocity scaling mechanism.

$$\mathbf{U}_i(t + \Delta t) = \mathbf{U}_i(t + \Delta t) r_{KE}(t + \Delta t) \quad (2.71)$$

2.5. Effective Zone of Influence, Influence Number and Number of Effective Molecules Factor

In nature, all particles interact with each other. However, increasing distance between particles leads the attraction force to be very small and the potential converges asymptotically to zero as can be observed in Figure 2.1. In order to decrease the CPU time required for simulation, a cut-off radius, R_{zone} , can be determined and the interaction of particles can be neglected outside of this zone. Corresponding volume is referred as the effective zone of influence.

As Çıray proposed [1], omitting the initial velocities which has no effect on instantaneous interaction force, total interaction outside a zone with diameter, R , of influence can be related by referencing the center of any particle:

$$U_i^2(r) = \int_R^{\infty} -2\pi r s \psi(r) dr \quad (2.72)$$

Note that, Eqn. 2.72 is defined in non-dimensional form and 2-D space. The non-dimensional L-J potential, given in Eqn. 2.55, can be utilized. Since only a weak attraction is observed outside of the effective zone, the repulsion term (12th power) can be omitted also. Furthermore, assuming the particles to be distributed uniformly, particle density, i.e. ρ , in any sample of area is considered to be the same.

$$U_i^2(r) = 2\pi\rho \int_R^{\infty} r \frac{1}{r^6} dr = \frac{\pi\rho}{2R^4} \quad (2.73)$$

$$|U_i(R_{zone})| = \sqrt{\frac{\pi\rho}{2}} R_{zone}^{-2} \quad (2.74)$$

$$|U_i(1)| = \sqrt{\frac{\pi\rho}{2}} \quad (2.75)$$

The influence number, I , is defined as the ratio of the effect of interaction outside effective the zone, given in Eqn. 2.74, to all interaction effects, provided in Eqn. 2.75. Therefore, the influence number in two-dimensional space is given in Eqn. 2.76 while three-dimensional projection of the influence number is presented in Eqn. 2.77.

$$I_{2D} = \frac{|U_i(R_{zone})|}{|U_i(1)|} = R_{zone}^{-2} \quad (2.76)$$

$$I_{3D} = \frac{|U_i(R_{zone})|}{|U_i(1)|} = R_{zone}^{-3} \quad (2.77)$$

The number of effective molecules factor, i.e. $NEMF$, is the ratio of the number of particles in the effective zone to the number of total particles. When the particles are assumed to be distributed uniformly, $NEMF$ is the ratio of the volume of the effective zone over the total volume of the system.

In simulations, the effective zone of influence is taken as three times of the diameter, in other words $R_{zone} = 6$. Also, each system is placed into a cube with edges, L , to be

equal to the 93 times of the diameter. Using this data, the influence number and the number of effective molecules factor are calculated in Eqn. 2.78 and Eqn. 2.79, respectively.

$$I = \frac{|U_i(R_{zone})|}{|U_i(1)|} = \frac{1}{6^3} = \frac{1}{216} = 0.46\% \quad (2.76)$$

$$NEMF = \frac{\text{effective volume}}{\text{total volume}} = \frac{\frac{4}{3}\pi R_{zone}^3}{L^3} = \frac{\frac{4}{3}\pi 6^3}{93^3} = 0.11\% \quad (2.77)$$

Analysis of the results shows that by using the effective zone of influence, even if 0.11% of total particles are used in simulations, only 0.46% of the total effect is neglected.

2.6. Interaction Between Unlike Molecules

In simulations where the interaction of two dissimilar non-bonded atoms takes place, the potential energy definition in Eqn. 2.40 is still valid thanks to the combining rules. Although there are many alternatives, discussed in Section 1.3, Lorentz-Berthelot Combination Rule is applied taking its ease of implementation into consideration.

$$\sigma = \frac{\sigma_i + \sigma_j}{2} \quad (2.78)$$

$$\varepsilon = \sqrt{\varepsilon_i \varepsilon_j} \quad (2.79)$$

CHAPTER 3

IMPLEMENTATION PROCESS OF THE THEORY

3.1. Introduction

This chapter describes the implementation process of the theory, provided in Chapter 2, as a set of simulation codes. First, the flow chart of the program is presented. The program consists of main code and its subroutines, which are also explained in the scope of this chapter. Subroutines are divided into five categories according to their functions as definition of initials, boundary control, analysis, visualization and reporting subroutines. In order to prepare the program and run the simulation, MATLAB R2018a programming language and computing environment is used.

3.2. The Flow Chart

The flow chart of the simulation process is presented in Figure 3.1. There exist the main code and subroutine calls. Definition of initials and boundary control subroutines are called during iterations and colored in green. After iterations; analysis subroutines, colored in blue, are called in order to make investigations on the desired phenomenon. Finally; visualization and reporting subroutines, colored in purple, prepare the outputs of the simulation.

In the main program; simulation parameters such as duration, time-step, effective zone of interaction, statistical and visualization selections, are assigned by the user first. Then the initial conditions are set. Number of systems, particles and matter specifications are made. Also, distances between the particles and clearances to the walls in any direction are selected by the user so initial positioning can be accomplished. Last, the user determines the flow velocity and system temperature of the particles.

After assignments for input data, “*define.m*” subroutine is called to create all required variables, perform initial positioning and velocity assignment of particles, make calculations such as the boundaries and reference total kinetic energy of the system.

Afterwards, iterations start for the specified duration and time-step loops. At the beginning each iteration, positions and velocities of previous iteration are assigned as initial conditions of the iteration. Then, another loop is created in order to check all possible interaction of particles. First, belonging systems of the particle pair are checked. If they belong to the same system, then the distance between particle centers is calculated. If particles are positioned inside their effective interaction zone, the velocity contributions to each other are calculated. When all possible interactions are examined, sum of velocity contributions are added to initial velocities of each particle.

The obtained velocities are rough velocities and needs to be scaled in order to control the total energy of the system. Therefore, the total kinetic energy in corresponding iteration is calculated based on rough velocities and the velocity scaling coefficient is calculated by dividing to the reference total kinetic energy. After that, velocities of particles are scaled by being multiplied by this coefficient.

Using the initial positions and the velocities after the interaction, boundary control of particles is performed. Path-wise motion of the particle is examined by “*bCheck.m*” subroutine. If any crossing at the boundaries is observed, elastic reflection of the particle is implemented, impact velocities to use for pressure calculations are collected and required update in velocity components and positions are made by “*bReflection.m*” subroutine. To calculate the pressure also in mid-planes, fictitious impacts of particles on imaginary mid-planes are also collected. If there is no wall crossing, calculated velocity components and positions are confirmed.

The procedure is repeated for each time-step loop until the final simulation time is reached. Then, database is ready for post-processing and analysis subroutines are called. In the scope of this work, “*tDiffusion.m*” and “*dVariation.m*” subroutines are

introduced in order to make thermal diffusion analyses and investigate the variation of density in unidirectional fluid flow, respectively.

Finally, visualization and reporting subroutines are called in order to prepare the outputs of the simulation. Visualization of states in iterations are created by "*tifVisualization.m*" subroutine. Results are being reported and desired figures are created by "*report.m*" subroutine.

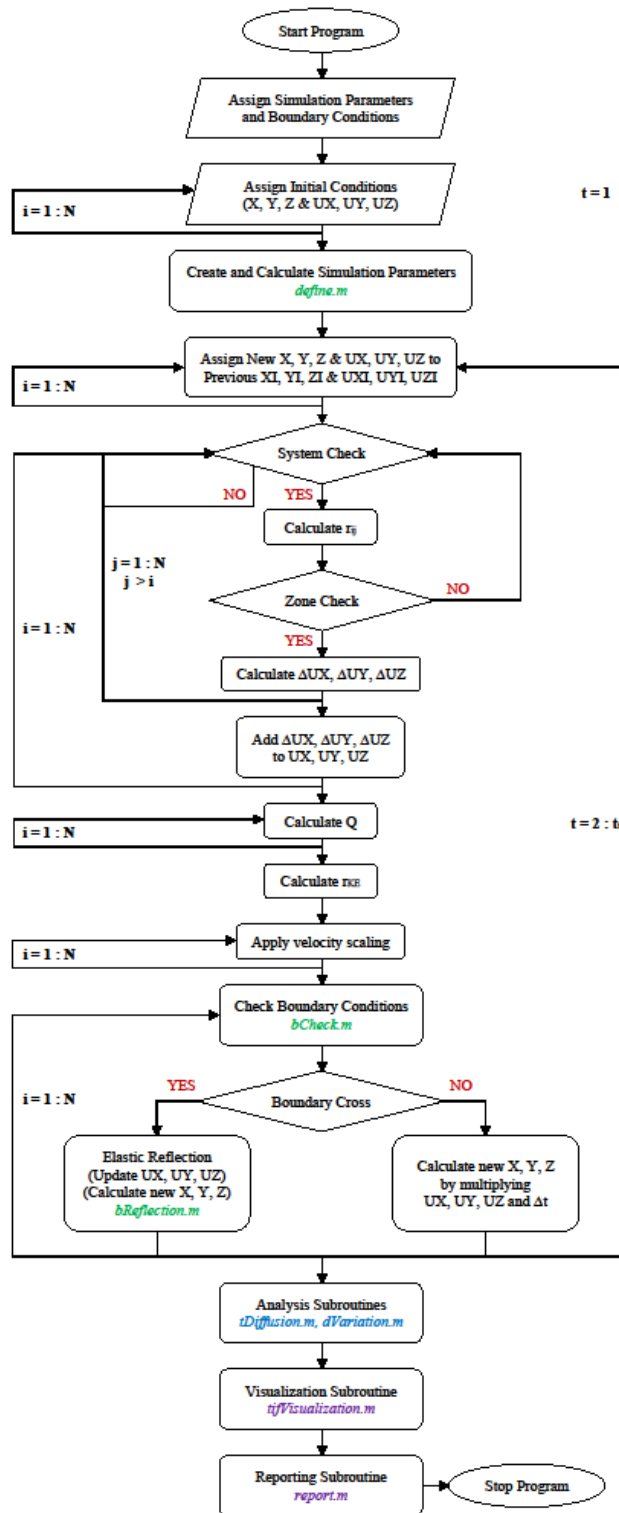


Figure 3.1. Flow Chart of the Simulation Process

3.3. The Main Code (*main.m*)

The main code is the executive part of the program. First; problem definition, simulation parameters selection, initial and boundary conditions are specified by the user. Afterwards, the main code performs the simulation and ensures the coordination among subroutines for tasks as defined in the flow chart. The main code calls subroutines in relation with each task for execution according to the process order. It provides the required inputs to subroutines and receives the outputs in order to use them in the simulation process. The main aim of using the main code with subroutine calls is to offer a flexibility in simulation capabilities. Simulation of a new application, analysis or problem is possible by modifying the current subroutine or introducing a new subroutine.

3.3.1. Problem Definition for an Application

Each application is labeled with a unique number. Once the application number is specified by the user, the main code calls appropriate subroutines developed for the application in simulation steps. Therefore; when a new application is introduced to the program, available appropriate subroutines can be utilized but development of additional subroutines may be required depending on the application needs.

3.3.2. Simulation Parameters

Simulation parameters should be determined in order to set the framework of the simulation. First of all, specification of particles should be made. Afterwards, simulation duration is specified. If there is any, phases of simulation should be determined. Furthermore, maximum allowed movement of particles at a reference velocity, given in *Table 2.2*, can be modified which is set 5% of the diameter as default. Likewise, advanced settings such as next potential estimation, data statistics and visualization output parameters can be changed or kept as default.

3.3.3. Initial and Boundary Condition Parameters

Initial set up and boundaries are created by the input of five parameters. If initial positioning is symmetric along each of axes, only the number of particles and the initial distance between centers arrays are requested along coordinate axes. Otherwise, initial position data matrix should be introduced. Initial motion is described by introducing the accompanying velocity due to the initial temperature and the system flow velocity. By default, the program randomly assigns velocity directions arising from thermal energy. However, initial directions set can also be introduced to the program. Boundary walls are created taking initial positioning data into consideration and adding wall clearances defined by the user.

3.3.4. Performing the Simulation

Once the database of simulation is created, all possible interactions between particles are checked for each time-step and contributions are calculated in terms of velocity first. Then velocity contributions are added to the initial velocity of each particle. Next, total kinetic energies of systems are calculated and corresponding velocity scaling coefficients are determined. After scaling, final velocities are obtained.

3.4. Subroutines

Subroutines are introduced in order to fulfill definition and creation of simulation initials, control of boundaries, statistical analysis, visualization and reporting duties. This section is devoted to provide detailed information about the solutions to fulfill these duties.

3.4.1. Definition of Initials Subroutine (*define.m*)

This subroutine is mainly responsible for definition of simulation variables and creation of initial set up of particles and surrounding boundaries.

3.4.1.1. Definition of Simulation Variables

According to user preferences in the main code, dimensions of simulation variables are determined. Furthermore, definition of variables is made on this basis before being delivered to the main code. Some important examples to these variables are the time-step, number of simulation iterations, total number of particles and their final velocity and position data variables, system potential and kinetic energy data variables, kinetic energy scaling coefficient and boundary pressure data variables.

3.4.1.2. Creation of Initial Set Up of Particles and Surrounding Boundaries

Once initial and boundary condition parameters are assigned as described in Section 3.3.3, the subroutine uses these input values to create the position matrix of particles. Afterwards; applying wall clearance constraints, boundary matrices of systems are created. Also, direction of initial velocities, in proportion to the temperature of the particle, are assigned randomly. The relation between the average temperature of N particles, T , and resultant kinetic energy is described by the Boltzmann relation, given in Eqn. 3.1.

$$\frac{3}{2}k_bT = \frac{1}{2}m \sum_{p=1}^N U_p^2 \quad (3.1)$$

where k_b is the Boltzmann constant and U_p is the corresponding velocity of particles. Temperature, i.e. excitation speed, of each particle is visualized according to “jet colormap array” of MATLAB. Color scheme of the array is provided in Figure 3.2. Dark blue color tones express low speeds while dark red color tones are used to represent high speeds.



Figure 3.2. Jet Colormap Array

As an example, an initial set up consisting of two separated systems at different temperatures and enclosing 1000 particles each, is visualized in Figure 3.3.

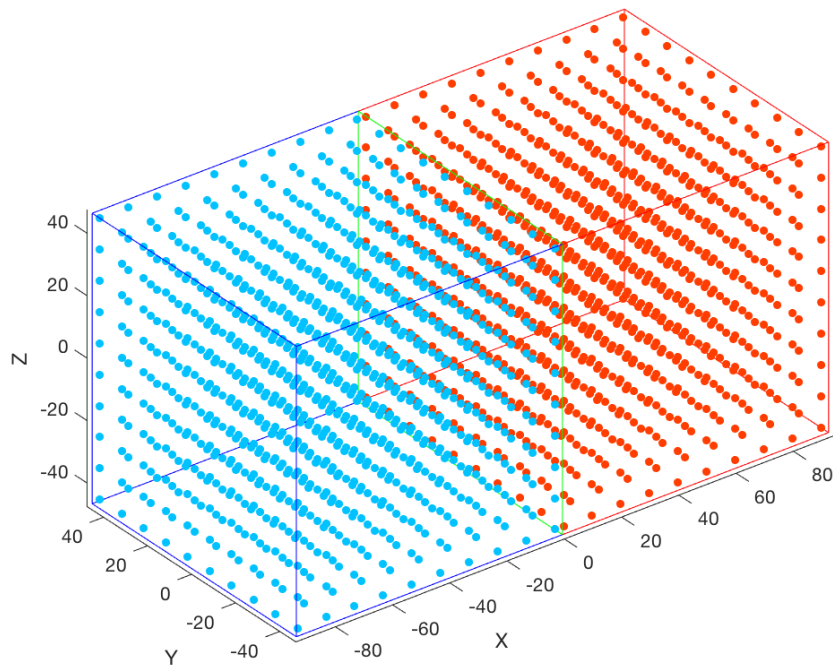


Figure 3.3. Initial Set Up for Two 1000-Particle Systems

3.4.2. Boundary Control Subroutines

Boundary control of particles is accomplished by two subroutines. Destination positions of particles are checked after interacting with other particles in the system during each time-step first. For particles experiencing boundary cross out of the system, elastic reflection from the boundary surface is assumed. Impact of particles on each boundary surface is recorded in order to calculate the pressure of the system. In order to make a further check on system pressure, imaginary surfaces are defined at the center of each system. Associated speeds passing through these imaginary surfaces are also collected to calculate the pressure.

3.4.2.1. Checking Destination Positions of Particles (*bCheck.m*)

After the calculation of final velocities as described in Section 3.3.4, position destination of each particle is checked with respect to system boundaries. An example is given in Figure 3.4.

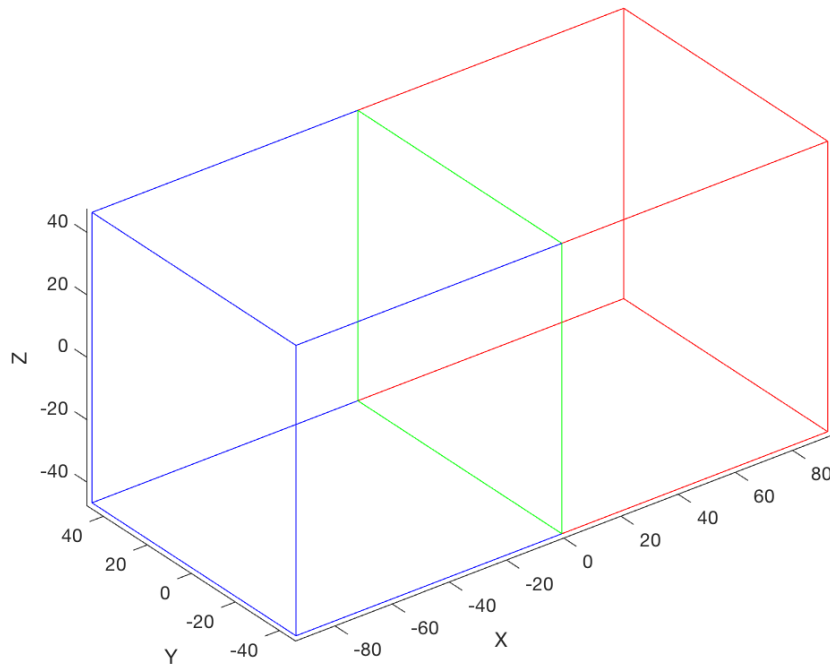


Figure 3.4. Separated System Boundaries

The idea is to create an array possessing number of elements equal to the number of faces of each system. For each particle in each system, boundary cross check is performed and the corresponding face element of the array is updated as 1 or 0 with respect to experience a boundary cross or not.

3.4.2.2. Elastic Boundary Reflection (*bReflection.m*)

If the summation of all elements in the boundary cross check array is different to zero, it means that the particle experiences boundary cross. In these cases, elastic reflection condition is applied.

Boundary check and reflection subroutines are called in the same loop in order to decrease memory requirements. Only total number of boundary impacts data is collected for each time iteration of the simulation as a statistical data.

3.4.2.3. Updates on Position and Velocity Components in Case of a Reflection (*bReflection.m*)

In case boundary cross happens, calculation on elastic reflection basis is achieved by mirroring the initial position and velocity vector of the particle symmetrically along the impacted boundary planes and adding the displacement during the time iteration based on this updated data. In Figure 3.5, the method is explained for a particle (represented as plain-blue) experiencing two boundary crosses at the corner. The particle moves along the velocity vector which is shown as blue array. The destination position of the particle at the end of time-step is calculated as blue dashed position. Since destination position crosses through two surfaces, the solution is to mirror the initial position and velocity vector along in both surface axes. The position and velocity vector to be used in calculating the correct destination of particle are represented in dashed-green. Then the final position and velocity vector of the particle are obtained under elastic reflection assumption.

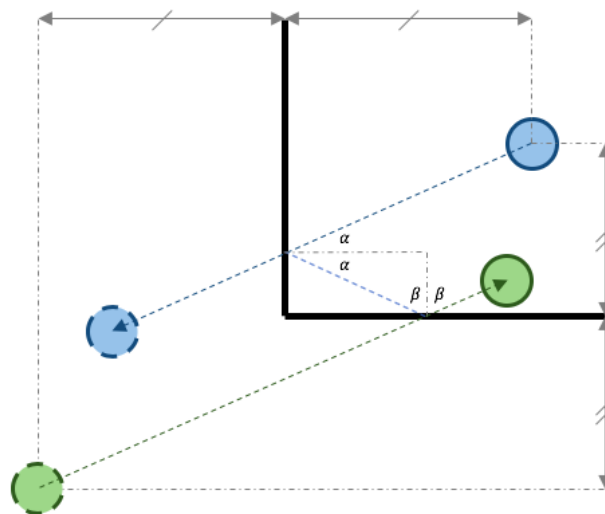


Figure 3.5. Velocity and Position Updates for Boundary Crosses at the Corner

3.4.2.4. Impacts at Boundaries and Mid-Planes (*bReflection.m*)

On each boundary surface, total impact of particles is calculated as also which is also mentioned in Section 3.4.2.2. Additionally, impacts on imaginary mid-planes of the system are summed for each time iteration in order to make further check related to pressure results obtained by the simulation. For the example given in Figure 3.4, mid-planes of two systems are added in Figure 3.6, enclosed with dashed lines.

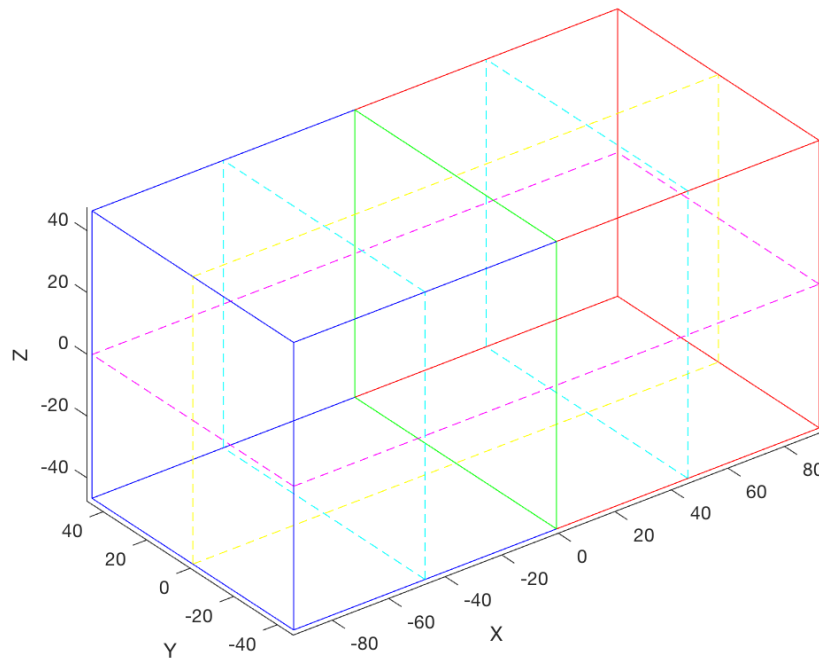


Figure 3.6. Boundary and Mid-Planes where Impacts are Checked

3.4.3. Analysis Subroutines

Calculation of final position and velocities of particles and collecting data of states, any desired analysis can be made related to the problem. Subroutines for thermal diffusion and density variation analyses are prepared in the scope of the thesis. However, it is possible to introduce additional subroutines for more analyses such as mean free path, velocity profile or wave number.

3.4.3.1. Thermal Diffusion Analyses (*tDiffusion.m*)

Thermal diffusion analyses include average temperature calculations in terms of two different tags: initial system tag and current volume tag. Initial system tag is determined at the start of the simulation for particles according to their belonging initial system and stays as it is until the end of the simulations. Current volume tag is checked in every time iteration because it tags particles according to their instant involvements in the volume of initial systems by using the position data. Changes of average temperature from these two perspectives are determined.

Additionally, an analysis is made on the thermal conductivity coefficient. Defining smaller cubes inside boundaries, average temperature of each box is calculated in each time iteration. Using the previous and current average temperature of cubes, diffusion of thermal energy is observed and thermal conductivity of the particle is calculated.

3.4.3.2. Density Variation Analysis (*dVariation.m*)

Density variation analysis is performed for the unidirectional fluid flow application. First, the system is divided into small cubes and the particles are tagged according to their instantaneous positions in these cubes. The subroutine calculates the number of particles in each box and classifies them according to the occupied densities.

3.4.4. Visualization Subroutine (*tifVisualization.m*)

After analyses are performed, visualization subroutine is called if the visualization frequency parameter is set by the user. The subroutine visualizes the boundaries, particle positions and boundaries in a “tif” formatted document for each time iteration. As issued in Section 3.4.1.2, jet colormap which is given in Figure 3.2, is used to describe the temperature and corresponding speed of the particle due to its thermal energy. Visualization structure is exemplified in Figure 3.3.

3.4.5. Reporting Subroutine (*report.m*)

Within this subroutine, the main goal is to provide and compare results. Statistical, mean or summation results are calculated. Furthermore, nondimensionalized

parameters are converted to their dimensional form. Moreover, theoretical values related to analyses are calculated and compared with simulation results in charts or tables.

CHAPTER 4

RESULTS

4.1. Introduction

In this chapter, simulation results are presented and discussed for thermal diffusion and unidirectional fluid flow applications. In addition, some remarks for the time-step dependence and the time efficiency of simulations are made.

4.2. Thermal Diffusion Simulation

Two particle systems are introduced, possessing Argon particles at 120 Kelvin and 300 Kelvin as visualized in Figure 3.3. There are two compartments for the two systems, named as compartment-1 for the system at 300 Kelvin and compartment-2 for the system at 120 Kelvin. Ten particles in each direction, i.e. 1000 particles, are initially positioned in each compartments having the same distance between the particle centers which is equal to ten times of one particle diameter along coordinate axes. The clearance of side particles with the boundary surfaces is set as the one particle diameter. System boundaries are created based on initial positioning parameters as shown in Figure 3.4. Note that, there is a separation surface represented with green lines, preventing the interaction and mixing of particles of the two compartments. In each system, particles are initially assigned the same average velocity represented by the blue and red colors for corresponding system temperature values of 120 and 300 Kelvin respectively. The reason behind to select 120 Kelvin and 300 Kelvin is to be able to compare the results with the previous simulations, performed by Eneren [2]. Directions of the velocity arising due to the thermal energy of particles are assigned randomly.

The thermal diffusion simulation is divided into two phases and performed approximately for 3000 picoseconds. In the first phase (phase-1), particles are allowed

to interact only with the same system particles for 1000 picoseconds. In that phase, both systems are expected to reach their equilibrium states. The second phase (phase-2) is also called as the mixing phase, where there is no separation and thermal energy is able to diffuse via motion of particles. The duration of the mixing phase is taken as 2000 picoseconds. Due to the removal of the separation, mixing phase of the simulation is continued for only one system defined by outer surfaces which is visualized in Figure 4.1.

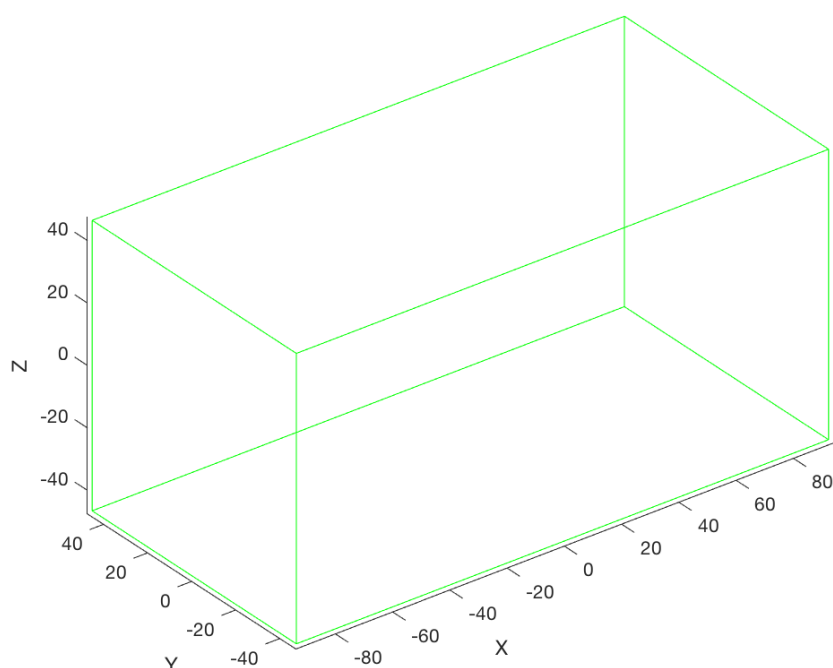


Figure 4.1. The System Boundaries During Phase-2

4.2.1. Investigation of Equilibrium State in Phase-1

Establishment of equilibrium state in phase 1 is checked by the total potential energy between system particles, statistical values of speed and velocity components also the distributions and impact pressures at boundaries and system mid-planes.

4.2.1.1. From Energy Perspective

One indicator of equilibrium is the potential energy of the system. In equilibrium state, zero potential energy is expected. For each system, potential energy change during non-dimensional (n.d.) simulation steps of phase-1 is given in Figure 4.2 and Figure 4.3.

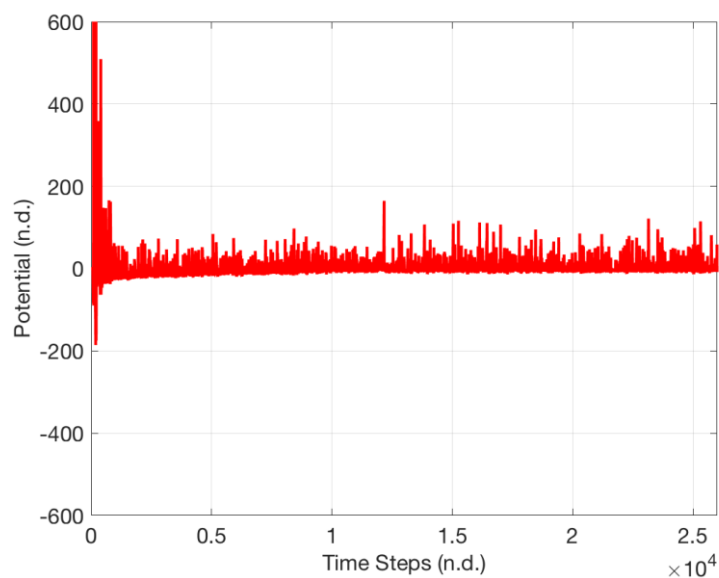


Figure 4.2. Total Potential Energy in Compartment-1 at 300 Kelvin (Phase-1)

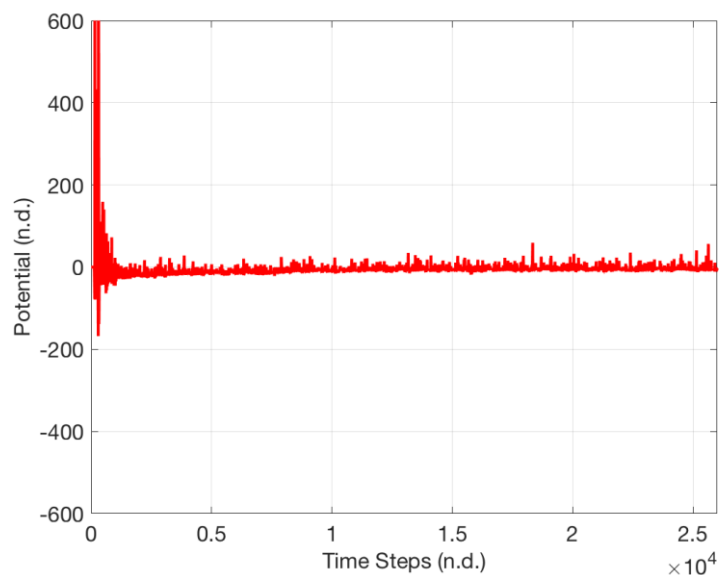


Figure 4.3. Total Potential Energy in Compartment-2 at 120 Kelvin (Phase-1)

Both systems seem to reach the equilibrium state, i.e. zero potential value, in similar time period. Comparing the simulation results obtained from previous work [2], higher fluctuations are observed from zero potential. This is an expected result because collision of particles is only considered to bring colliding particles at a distance exactly equal to the equilibrium distance in the previous work. Disturbances due to collisions are also included and modeled in this thesis according to the Lennard-Jones potential model. Furthermore, fluctuations for the system at 300 Kelvin is higher than the system at 120 Kelvin. This is also foreseeable, considering the increase in kinetic energy to yield stronger collisions.

As explained in Section 2.4, kinetic energy in the system is controlled with velocity scaling method. Calculated velocity scaling coefficient data is presented for two compartments in Figure 4.4 and Figure 4.5.

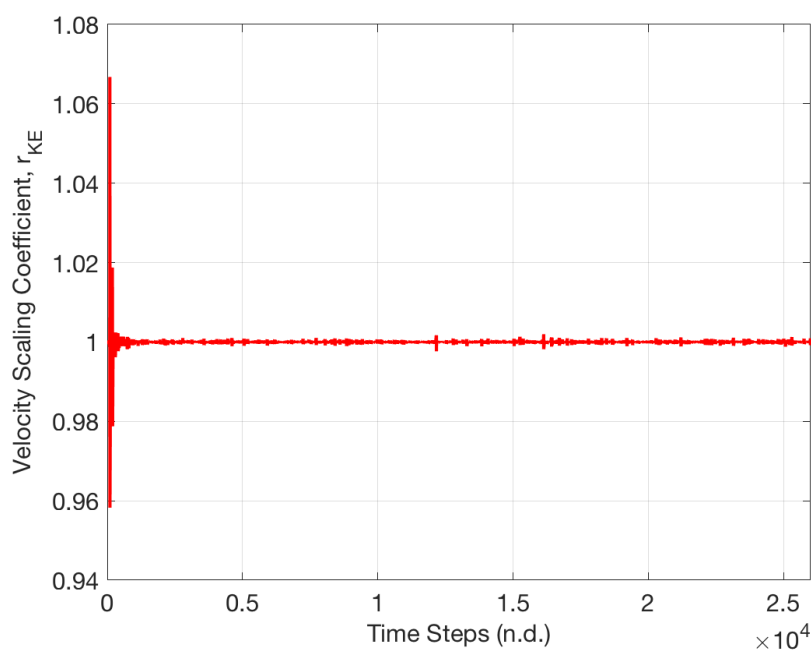


Figure 4.4. Velocity Scaling Coefficient in Compartment-1 (Phase-1)

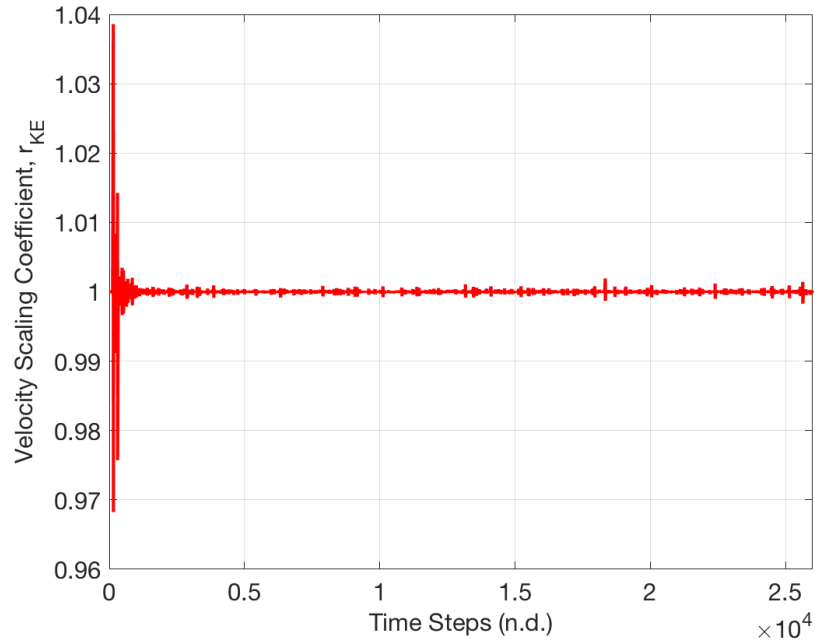


Figure 4.5. Velocity Scaling Coefficient in Compartment-2 (Phase-1)

After a short transition period, velocity scaling coefficients converge to the expected value, 1. Compared to Eneren's results [2], fluctuations in velocity scaling coefficient is decreased from 40% to 11%. This is one indicator of the success thanks to the improvement applied to the method.

4.2.1.2. Associated Speeds and Speed Distributions

The most probable, the average and the root mean square speeds are defined as associated speeds. They are formulated for ideal gases as given in Eqn. 4.1, Eqn. 4.2 and Eqn. 4.3 respectively.

$$U_{mps} = \sqrt{\frac{2RT}{M}} \quad (4.1)$$

$$U_{ave} = \sqrt{\frac{8RT}{\pi M}} \quad (4.2)$$

$$U_{rms} = \sqrt{\frac{3RT}{M}} \quad (4.3)$$

where R is the Universal Gas Constant, M is the molar mass of the gas and T is the system temperature. Comparison of simulation results obtained by improved method and original method [2] with theoretical data is made in *Table 4.1*. The effect of improvement in accuracy is observed.

Table 4.1. *Comparison of the Associated Speeds Results*

Data Source	T_{ave} [K]	U_{mps} [m/s]	U_{ave} [m/s]	U_{rms} [m/s]
Theoretical		353.4	398.8	432.8
Original	300	346.0 (+2.10%)	389.8 (-2.26%)	432.9 (+0.03%)
Improved		353.4 (0.00%)	398.8 (0.00%)	432.8 (0.00%)
Theoretical		223.5	252.2	273.8
Original	120	228.1 (+2.06%)	250.2 (-0.79%)	273.9 (+0.03%)
Improved		223.5 (0.00%)	254.0 (+0.71%)	273.7 (-0.03%)

Furthermore, the distribution of speeds should coincide with the Maxwell-Boltzmann distribution at equilibrium state. The probability density function of the Maxwell-Boltzmann distribution is given in Eqn. 4.4.

$$f(U) = 4\pi U^2 \left(\frac{m}{2\pi k_b T} \right)^{\frac{3}{2}} e^{-\frac{mU^2}{2k_b T}} \quad (4.4)$$

where k_b is the Boltzmann constant, U is the speed of the particle, m is the mass of the particle and T is the system temperature. Simulation speed distributions, i.e. probability density functions, at the end of phase-1 (1000 picoseconds) are represented in Figure 4.6 and Figure 4.7.

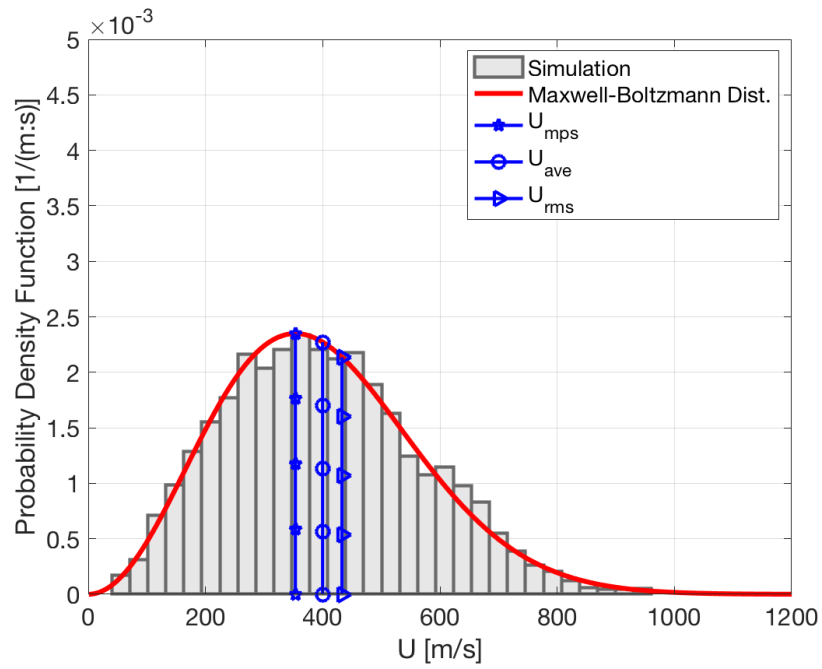


Figure 4.6. Speed Distribution in Compartment-1 (at 1000 ps, end of Phase-1)

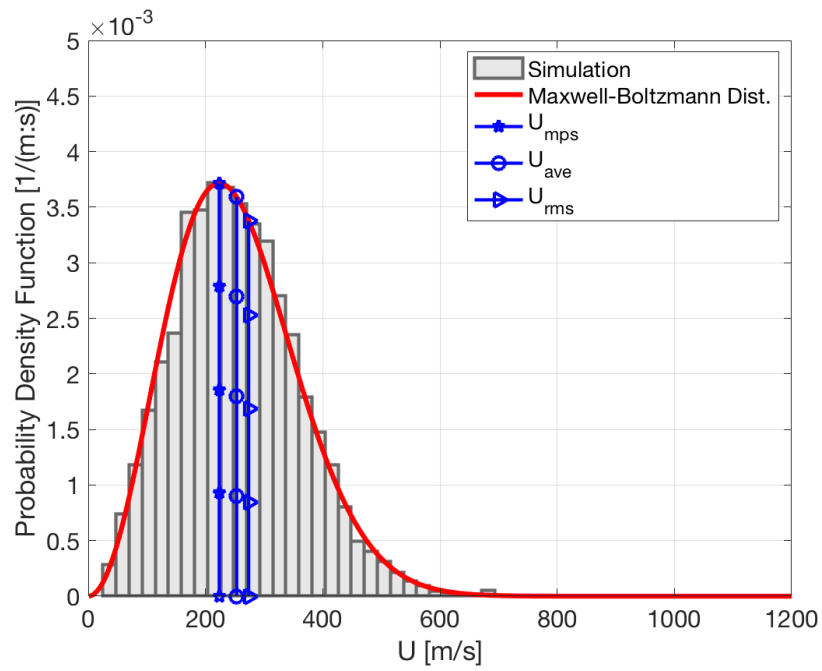


Figure 4.7. Speed Distribution in Compartment-2 (at 1000 ps, end of Phase-1)

Satisfying consistence to Maxwell-Boltzmann is achieved. In addition, the results fit slightly better than the original method [2].

In order to see the construction of the Maxwell-Boltzmann distribution, speed distributions at 100, 200 and 300 picoseconds are provided for the two systems in Figure 4.8 and Figure 4.9.

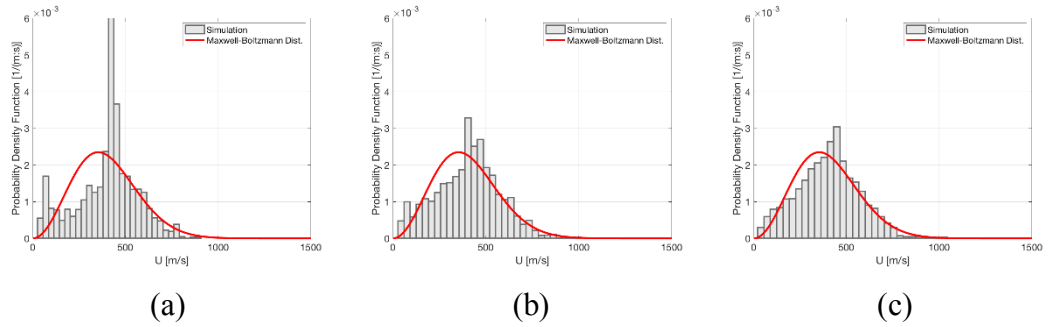


Figure 4.8. Speed Distributions in Compartment-1 at (a)100ps (b)200ps (c)300ps

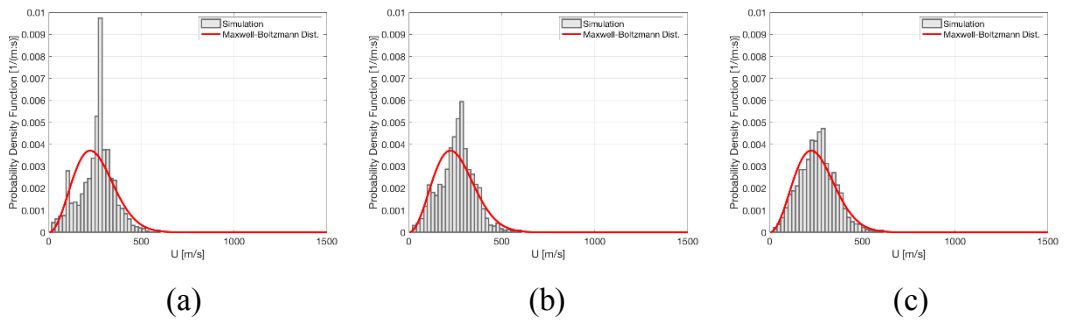


Figure 4.9. Speed Distributions in Compartment-2 at (a)100ps (b)200ps (c)300ps

Distribution of the velocity components is presented by standardized values, i.e. z-score, given in Eqn. 4.5.

$$z_x = \frac{U_x - \overline{U_x}}{\sigma_x} \quad (4.5a)$$

$$z_y = \frac{U_y - \overline{U_y}}{\sigma_y} \quad (4.5b)$$

$$z_z = \frac{U_z - \overline{U_z}}{\sigma_z} \quad (4.5c)$$

where $\overline{U_x}$, $\overline{U_y}$ and $\overline{U_z}$ accounts for the mean, σ_x , σ_y and σ_z denote the standard deviation of the velocity along corresponding coordinate axes.

As a result, Figure 4.10 and Figure 4.11 are obtained at the end of phase-1 from simulations which agree well with the Gaussian distribution.

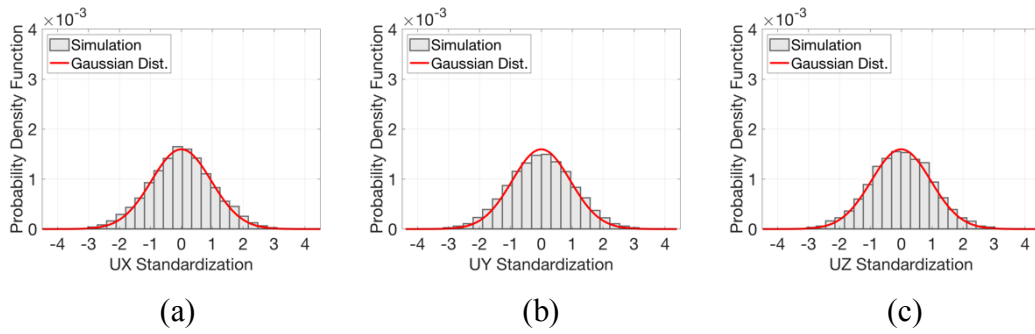


Figure 4.10. Profile of Velocity Components in Compartment-1 at the end of Phase-1 along (a)x (b)y (c)z axes

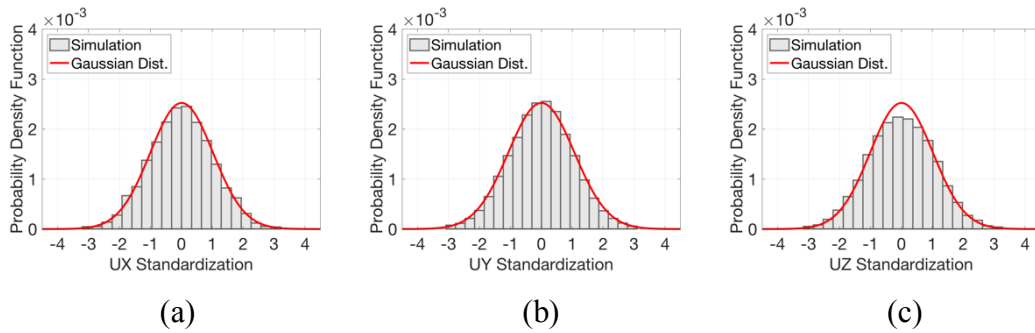


Figure 4.11. Profile of Velocity Components in Compartment-2 at the end of Phase-1 along (a)x (b)y (c)z axes

Similar to the construction of the Maxwell-Boltzmann distribution for speeds, the construction of the Gaussian distribution is also observed. The velocity distributions for both systems along x axis at 100, 200 and 300 picoseconds are used to present the construction of Gaussian distribution in Figure 4.12 and Figure 4.13.

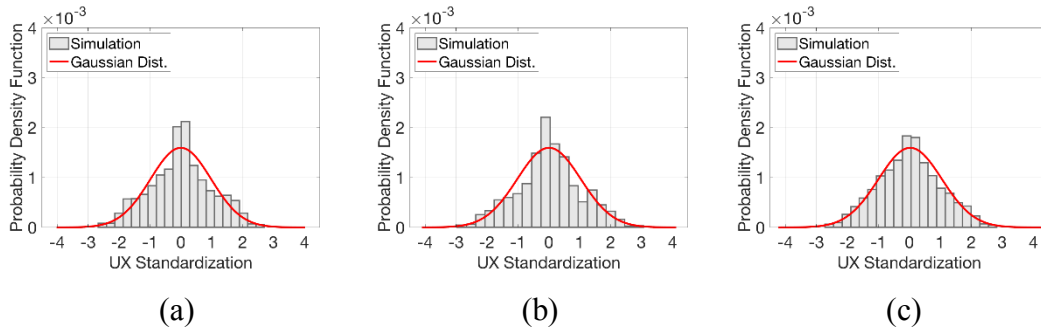


Figure 4.12. Profile of Velocity Components along x axis in Compartment-1 at (a)100ps (b)200ps (c)300ps

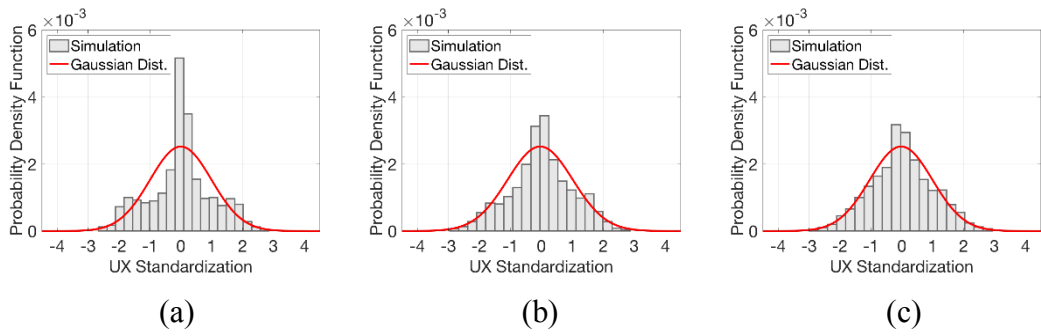


Figure 4.13. Profile of Velocity Components along x axis in Compartment-2 at (a)100ps (b)200ps (c)300ps

4.2.1.3. Pressures

The classical ideal gas equation, given in Eqn. 4.6, is used to calculate the theoretical pressures.

$$P = \frac{nRT}{V} = \frac{Nk_bT}{V} \quad (4.6)$$

where P denotes the pressure, n is the number of moles of the gas, R is the Universal Gas Constant, T is the system temperature, V is the system volume, N is the total number of particles possessed in the system and k_b is the Boltzmann Constant.

In order to describe the simulation results as pressure, two approaches are applied [2]. First approach is based on the particle speeds and the relation is provided in Eqn. 4.7.

$$P = \frac{\rho}{3} \sum_{i=1}^N U_i^2 \quad (4.7)$$

where ρ is the system density, U_i is the speed of each particle in the system. Second approach is to use the impulse and momentum change relations as given in Eqn. 4.8.

$$P = \sum_{t_1}^{t_2} \frac{m\Delta U}{A(t_2 - t_1)} \quad (4.8)$$

where m is the particle mass, ΔU is the magnitude of the change in velocity vector because of the impact, A is the corresponding surface area experiencing the impact, $t_2 - t_1$ is the elapsed time.

Pressures at boundary surfaces are calculated according to Eqn. 4.8 and tabulated in *Table 4.2*, referencing the normal directions of boundary surfaces given in Figure 3.4.

Table 4.2. Pressures at Boundaries (Phase-1)

T_{ave} [K]	-x dir. [kPa]	+x dir. [kPa]	-y dir. [kPa]	+y dir. [kPa]	-z dir. [kPa]	+z dir. [kPa]
300	127.03	127.97	134.51	134.33	131.19	127.21
120	54.93	53.55	49.01	47.16	54.57	52.60

Similar approach is applied to mid-planes as described previously in Figure 3.6. Results are presented in *Table 4.3*.

Table 4.3. Pressures at Mid-Planes (Phase-1)

T_{ave} [K]	x dir. [kPa]	y dir. [kPa]	z dir. [kPa]
300	128.67	133.60	129.01
120	54.02	48.86	53.89

Theoretical and simulation pressure data based on the two approach are presented in *Table 4.4*. Note that, the mean values of surface pressures are used in order to describe the system pressure.

Table 4.4. *System Pressures (Phase-1)*

<i>T_{ave}</i>	<i>From Ideal Gas Relation</i>	<i>From Velocity Squares</i>	<i>From Impacts at Boundary</i>	<i>From Impacts in Mid-Planes</i>
[K]	[kPa]	[kPa]	[kPa]	[kPa]
300	130.44	130.45	130.37	130.43
120	52.17	52.18	51.97	52.59

The simulation offers pressures generally in 1/10000 accuracy. Compared to the results in the original method [2], there is 100 times increase in average in terms of the pressure calculation precision.

4.2.2. Investigation of Equilibrium State and Thermal Diffusion in Phase-2

Similar to phase-1, same analyses are made in order to check the equilibrium state of the system. In addition, thermal equilibrium concepts and the diffusion rate of the thermal energy are investigated.

4.2.2.1. From Energy Perspective

The potential energy of the system in the mixing phase is calculated similar to the first phase. In Figure 4.14, zero potential energy is observed in the equilibrium state as expected.

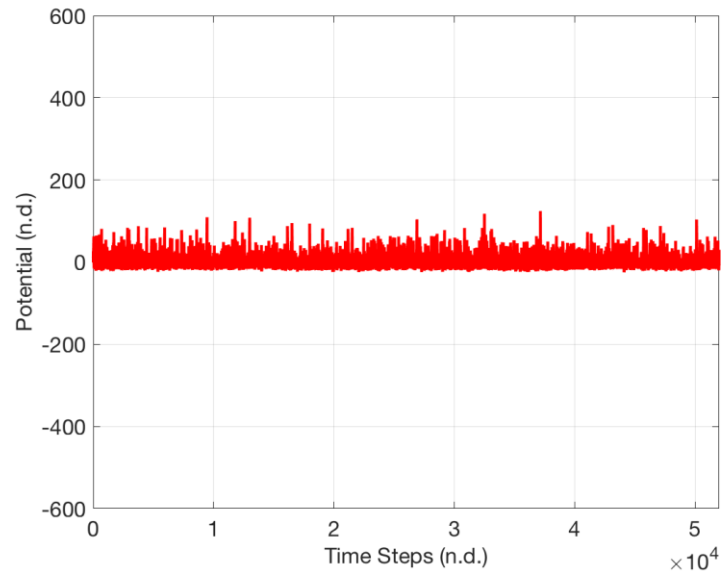


Figure 4.14. Total Potential Energy of the System (Phase-2)

Since the two systems were in the equilibrium state in terms of positions, no fluctuation is observed in terms of potential energy. Also, velocity scaling coefficient during the mixing phase is presented in Figure 4.15.

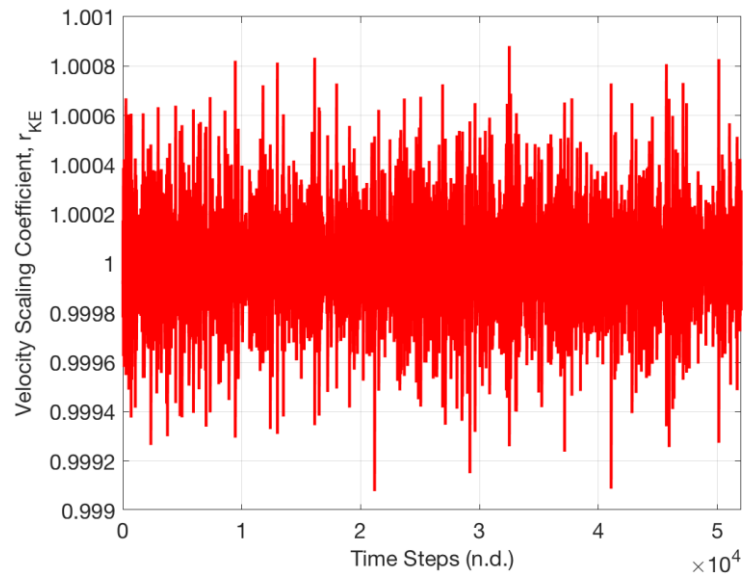


Figure 4.15. Velocity Scaling Coefficient of the System (Phase-2)

Note that, the range of the coefficient is very small and close to 1. Although the system is not in equilibrium in terms of the distribution of thermal energy, the overall system can be said to be in thermal equilibrium without mentioning the distribution.

4.2.2.2. Associated Speeds and Speed Distributions

Satisfactory simulation results are obtained again compared to theoretical data as shown in *Table 4.5*.

Table 4.5. Comparison of the Associated Speeds Results (Phase-2)

Data Source	T_{ave} [K]	U_{mps} [m/s]	U_{ave} [m/s]	U_{rms} [m/s]
Theoretical	210	295.7	333.6	362.1
Simulation		295.7 (0.00%)	332.6 (-0.30%)	362.1 (0.00%)

Simulation speed distributions, presented in Figure 4.16, again very close to the Maxwell-Boltzmann distribution.

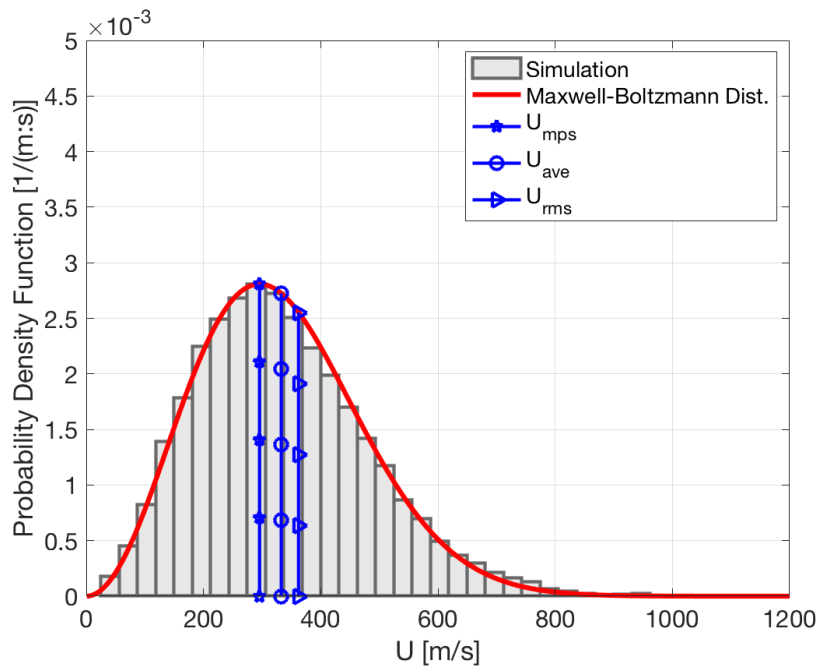


Figure 4.16. Speed Distribution of the System (Phase-2)

Velocity distributions along coordinate axes coincides with the Gaussian distribution in phase-2 also.

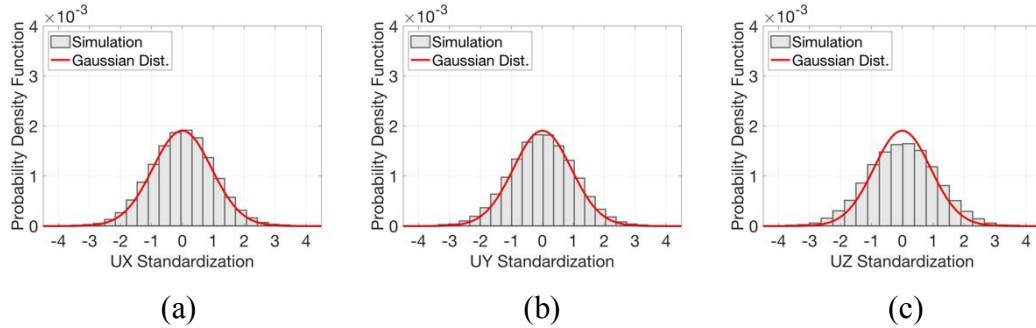


Figure 4.17. Velocity Components in Phase-2 along (a)x (b)y (c)z axes

4.2.2.3. Pressures

Theoretical and simulation pressure results are presented in Table 4.6. The simulation still offers satisfactory accuracy.

Table 4.6. System Pressures (Phase-2)

T_{ave} [K]	From Ideal Gas Relation [kPa]	From Velocity Squares [kPa]	From Impacts at Boundary [kPa]	From Impacts in Mid-Planes [kPa]
210	91.30	91.31	91.41	91.33

4.2.3. Investigation of Thermal Diffusion

In this section, visualizations of simulations are presented in respect of particle tracking and fixed volume bases. Furthermore, the thermal conductivity constant result is given with some remarks.

4.2.3.1. Particle Tracking Based Thermal Equilibrium

For the analysis, particles are tagged in respect of their initial system temperature. At the beginning, at two intermediate steps and at the end of the mixing phase, the states are presented in Figure 4.18, Figure 4.19, Figure 4.20 and Figure 4.21 respectively.

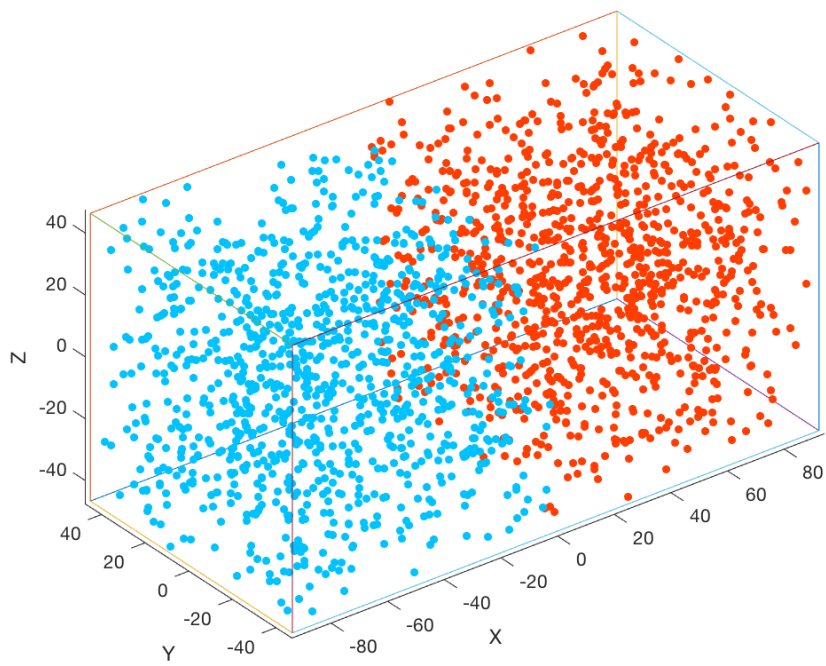


Figure 4.18. Initial Positions of Particles for Phase-2

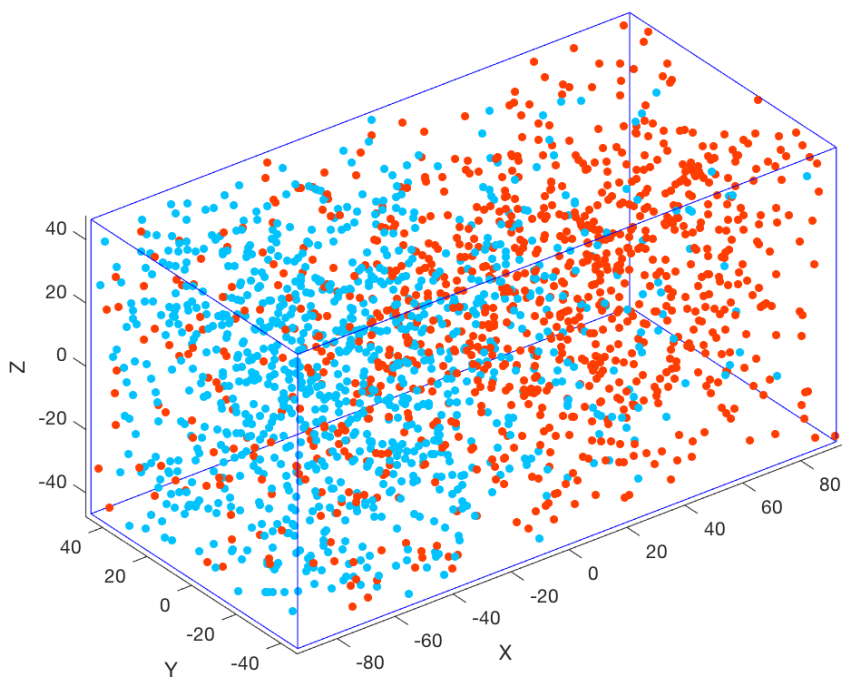


Figure 4.19. Positions of Particles after 100 Picoseconds in Phase-2

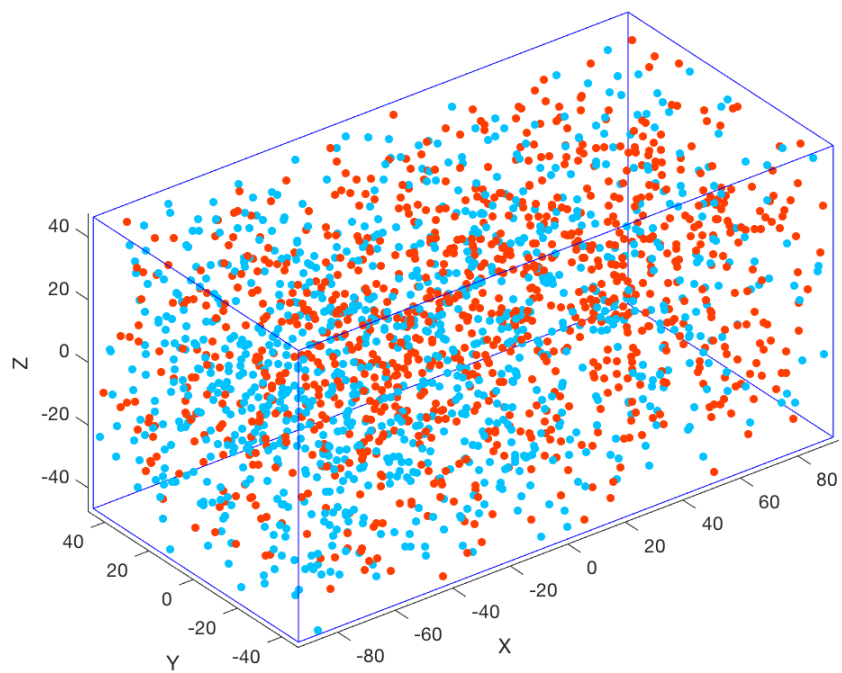


Figure 4.20. Positions of Particles after 200 Picoseconds in Phase-2

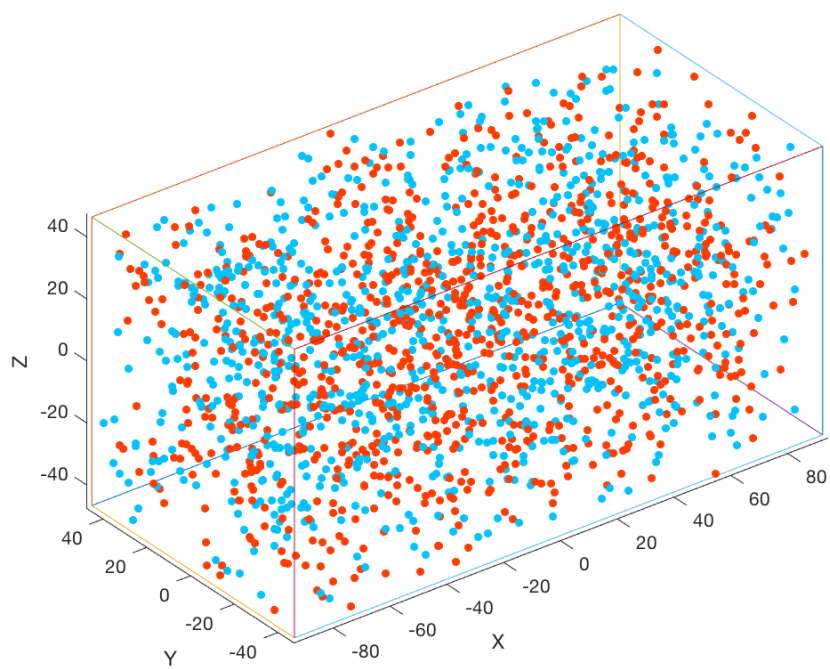


Figure 4.21. Final Positions of Particles after 2000 Picoseconds in Phase-2

As it can be indicated from Figure 4.19 and Figure 4.20, hotter particles diffuse to the colder compartment faster when the mixing phase is just started. Therefore, there is an increase in terms of density in that compartment at that time. In Figure 4.21, the particles of both systems are observed to mix well after some time. One interesting result is obtained when the average temperature of blue and red particle groups is calculated during phases of the simulation. Average temperature of the particle groups also reach a thermal equilibrium, which is given in Figure 4.22.

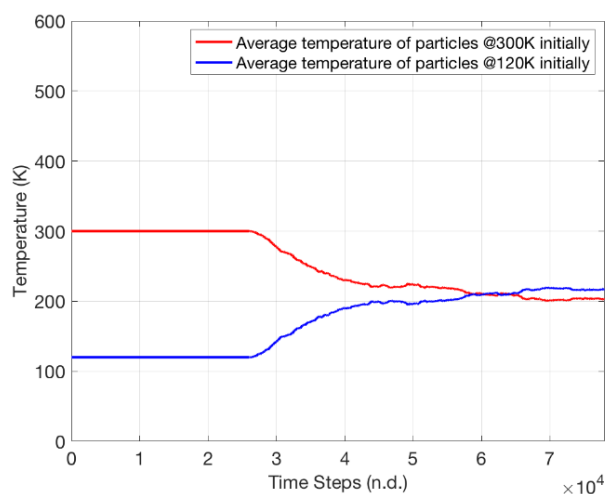


Figure 4.22. Average Temperature of Initial Particle Groups During Simulation

4.2.3.2. Fixed Volume Based Thermal Equilibrium

Another method to visualize the system is to use a color scale representing the velocity of particles. In the analysis; the jet colormap array, described in Figure 4.23, is used to describe the velocity or the kinetic energy of particles.

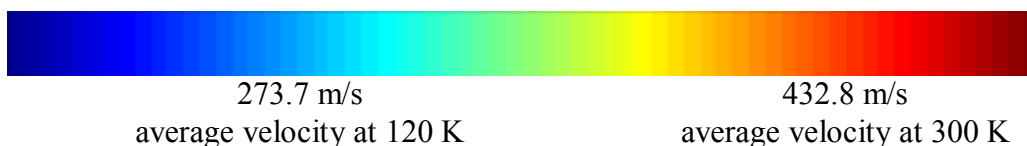


Figure 4.23. Jet Colormap Array to Describe Kinetic Energy of Particles

This time, locations are tagged in terms of the initial system volumes. At the beginning and at end of the mixing phase, the states are presented in Figure 4.24 and Figure 4.25.

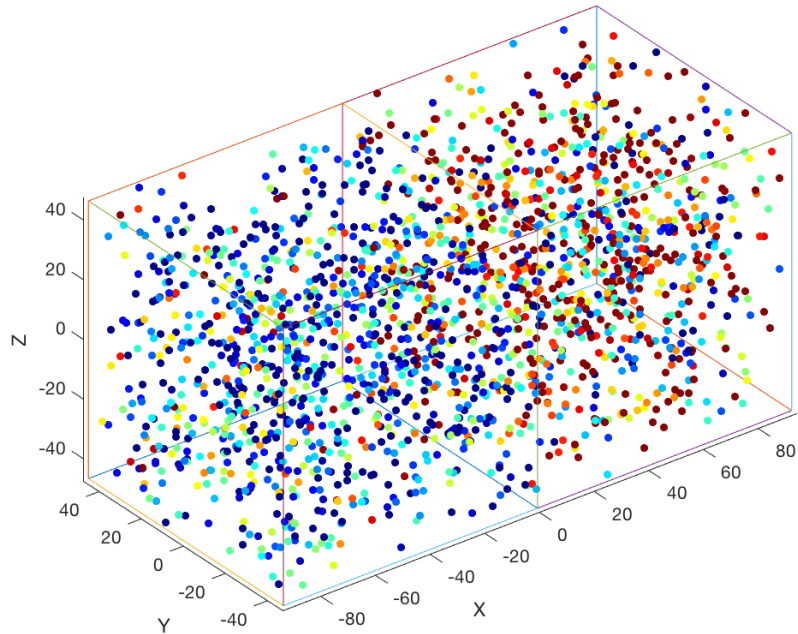


Figure 4.24. Initial Positions and Velocities of Particles for Phase-2

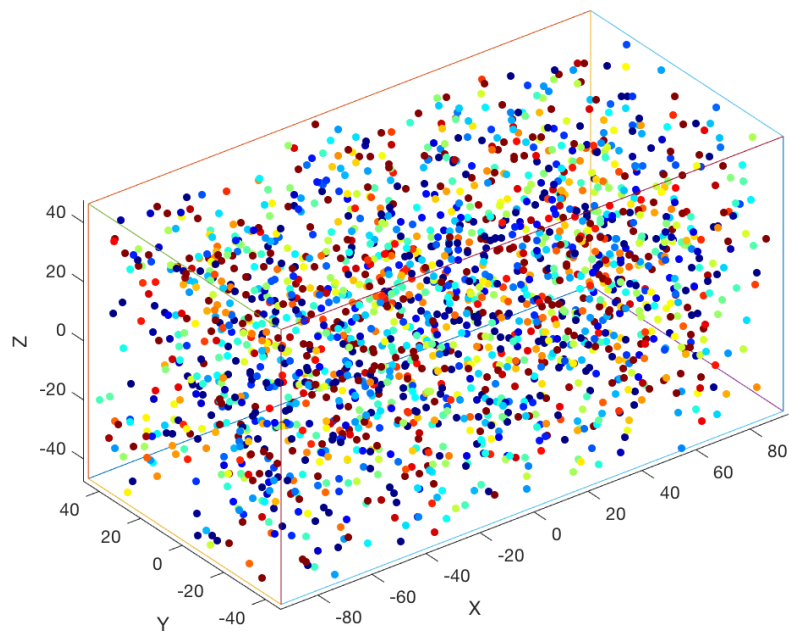


Figure 4.25. Final Positions and Velocities of Particles for Phase-2

Initially, red particles can be observed in the system kept at 120 Kelvin due to the Maxwell-Boltzmann distribution. Similarly, blue particles can be seen in the system kept at 300 Kelvin. However, the general color scheme is in blue tones for the system at 120 Kelvin. The general color scheme is also in red tones for the system at 300 Kelvin as expected.

In the final state, a new distribution is established but still in agreement with the Maxwell-Boltzmann distribution.

Another analysis is made for the average temperatures inside the boundaries of the two initial systems during phases of the simulation. The schematic of results is given in Figure 4.26, the data given in red and blue lines corresponds to compartment-1 and compartment-2 respectively.

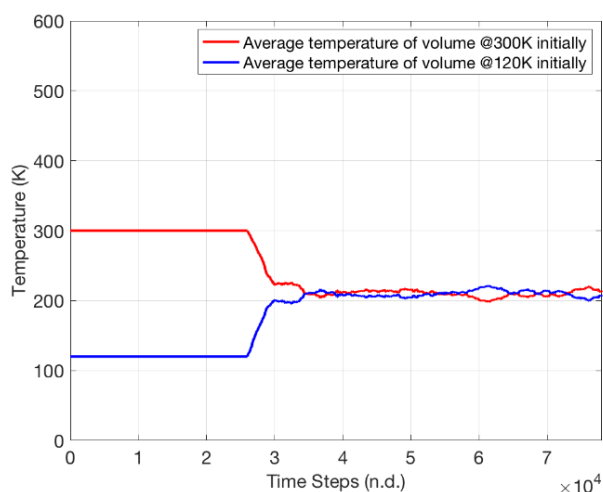


Figure 4.26. Average Temperature of Initial Compartments During Simulation

It is clear that diffusion of thermal energy takes place between the two sections of the new system until the same energy level is reached.

4.2.3.3. Calculation of Thermal Conductivity Constant

In order to calculate the thermal diffusion coefficient, the system is divided into cubical elements and average temperatures of particles in their coverage area is

calculated. Then compliance of the simulation results to the Heat Equation, presented in Eqn. 4.9, is checked.

$$\frac{\partial T}{\partial t} = \alpha \left(\frac{\partial^2 T}{\partial x^2} + \frac{\partial^2 T}{\partial y^2} + \frac{\partial^2 T}{\partial z^2} \right) \quad (4.9)$$

where T is the temperature of the system and α is the thermal diffusivity of the medium which is further described in Eqn. 4.10:

$$\alpha = \frac{k}{c\rho} \quad (4.10)$$

where k is the thermal conductivity of the material, c is the specific heat capacity and ρ is the mass per unit volume. Using the available data and simulation results, the average of thermal conductivity during the second phase of the simulation is calculated as 0.0115 Watts per meter Kelvin. Since the simulation is conducted with only 2000 particles, there exist some peak and minus values. This is because the number of particles is low for making such statistical analysis. When the peak and minus values are removed, i.e. results between 0 and 0.0400 are taken into consideration, corrected thermal conductivity is found as 0.0141 Watts per meter Kelvin. The data in literature is added to these results and tabulated in *Table 4.7*.

Table 4.7. Comparison of Thermal Conductivity Results with the Literature

k in Literature [W/mK]			k Results in Simulation [W/mK]	
At 100[K]	At 200[K]	At 300[K]	Average at 210 [K]	Corrected Average at 210 [K]
0.0062	0.0124	0.0179	0.0115	0.0141

4.3. Unidirectional Fluid Flow Simulation

The structure for unidirectional fluid flow simulations is visualized in Figure 4.27. For this application, periodic boundary condition is applied. The iterations are made only for the particles in the green region. Two surfaces, which have their normal vector along the x-axis, are let free for particles to pass through. Hence, the particle flow

along the x-axis is accomplished. Considering the continuity of the flow, when a particle just moves from the green section to the red section, it is logical to think another particle may be just arriving to the green section from the blue section in the same flow conditions. In simulations, the effective zone of influence is defined as the three times of the equilibrium distance. Therefore, the interactions of the particles in the cyan and magenta regions with other particles in the green section should be taken into consideration. Since the motion of the particles in these small regions are determined by the particles in the green section, the interactions are also included when the absolute value of distance in the x-axis between particles is more than the edge dimension of the cube along the x-axis minus the effective zone of influence.

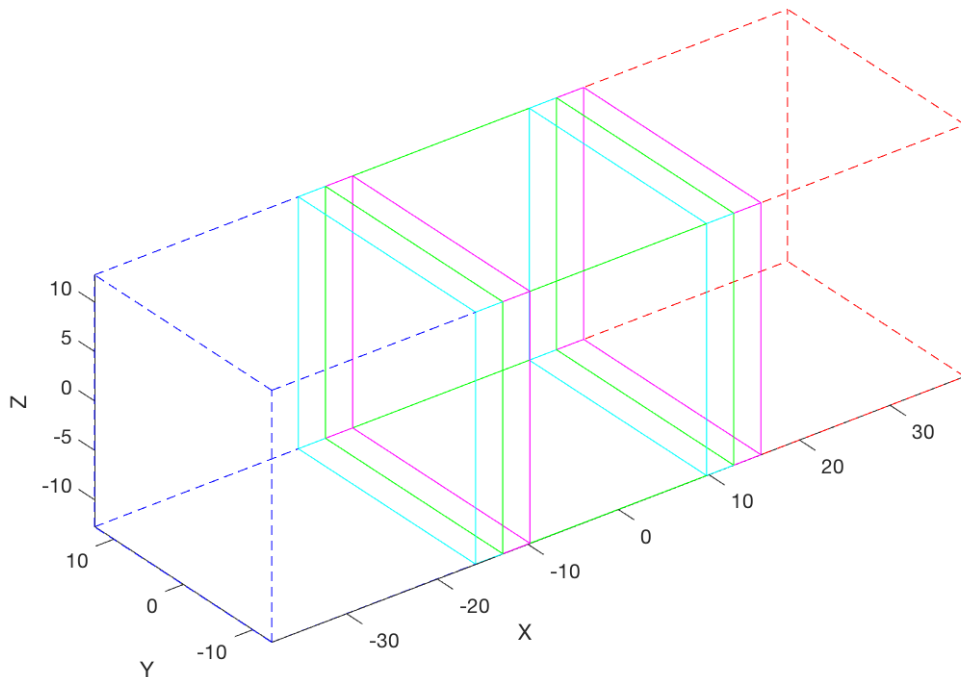


Figure 4.27. The Structure for Unidirectional Fluid Flow Simulation

As presented in Figure 4.28, ten Argon particles at 300 Kelvin are placed along each axis with 2.5 times of their diameter distance between the centers. 1000 Argon particles are obtained in total.

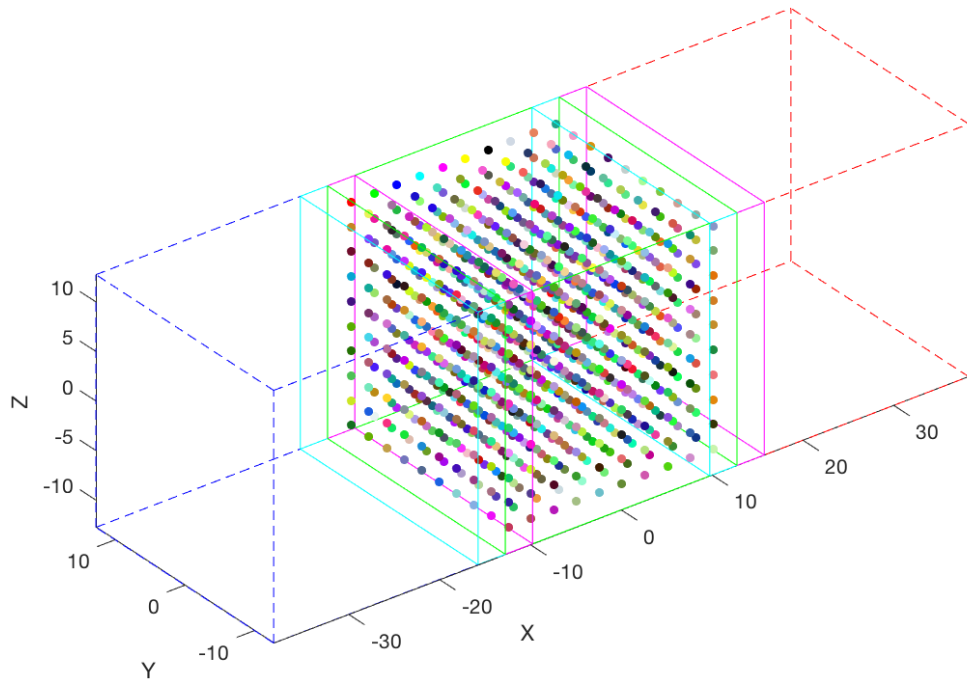


Figure 4.28. The Initial Setup for Unidirectional Fluid Flow Simulation

4.3.1. Variation of Density of Particles

Five simulation runs were performed for five test cases with different uniform flow velocities. Simulation duration is taken as 1000 picoseconds. Uniform flow velocities were taken along the x axis as 0.2, 0.5, 1, 2 and 5 times of the reference velocity of Argon, which was given in *Table 2.2*. As discussed in Section 2.5, increasing distance between particles leads the attraction force to be very small and the potential converges asymptotically to zero. Therefore, the concept of the effective zone of influence was introduced in this work. In order to investigate the variation of density of particles efficiently, this concept can be used again. Since the volume of the effective zone of influence is defined constant for all particles, the density around a particle is directly related to the total mass of parent particles in the zone. Using same particles in the system, which are all Argon, the density is related to the total number of parent particles in the zone.

The average number of particles in the effective zone of each one is 6.1 at 0.2 times of the reference velocity, which corresponds to 89 m/s. There are two particles, having the maximum density of 14 particles in their zone of influence which is shown in Figure 4.29.

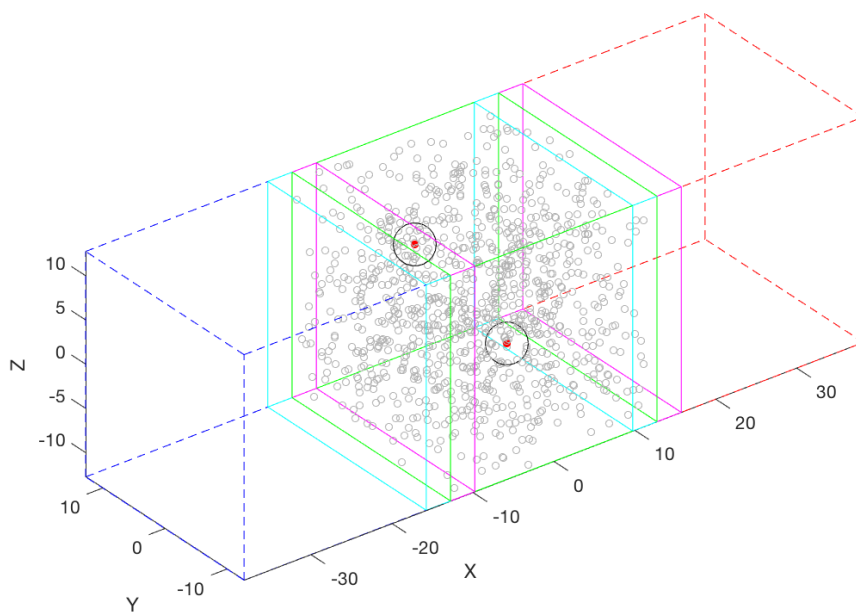


Figure 4.29. State of Particles at 0.2 Times of the Reference Velocity of Flow

The average number of particles in the effective zone of each one is 6.2 at 0.5 times of the reference velocity, which corresponds to 223 m/s. There are seven particles, having the maximum density of 13 particles in their zone of influence which is shown in Figure 4.30.

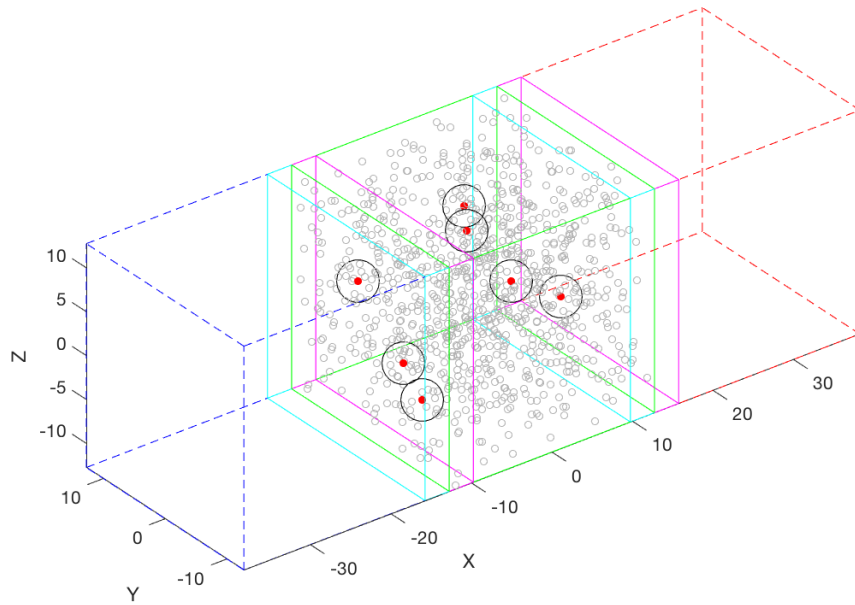


Figure 4.30. State of Particles at 0.5 Times of the Reference Velocity of Flow

The average number of particles in the effective zone of each one is 6.4 at the reference velocity, which corresponds to 447 m/s. There is one particle, having the maximum density of 16 particles in their zone of influence which is shown in Figure 4.31.

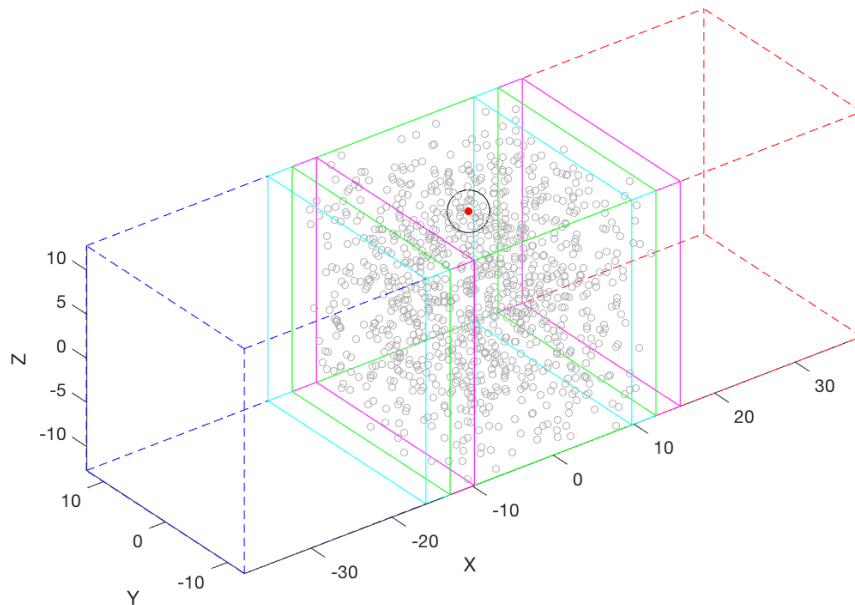


Figure 4.31. State of Particles at the Reference Velocity of Flow

The average number of particles in the effective zone of each one is 6.7 at 2 times of the reference velocity, which corresponds to 893 m/s. There are four particles, having the maximum density of 18 particles in their zone of influence which is shown in Figure 4.32.

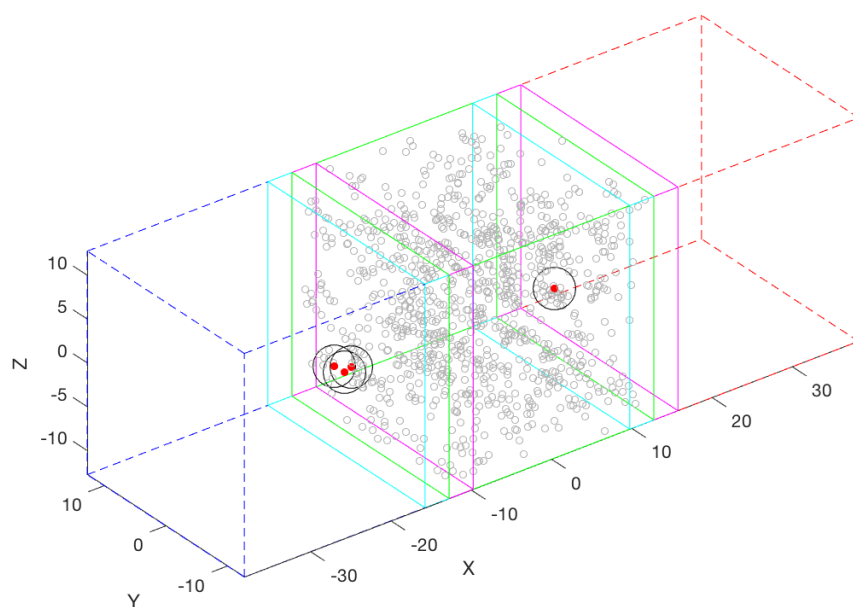


Figure 4.32. State of Particles at 2 Times of the Reference Velocity of Flow

The average number of particles in the effective zone of each one is 6.9 at 5 times of the reference velocity, which corresponds to 2233 m/s. There is one particle, having the maximum density of 24 particles in their zone of influence which is shown in Figure 4.33.

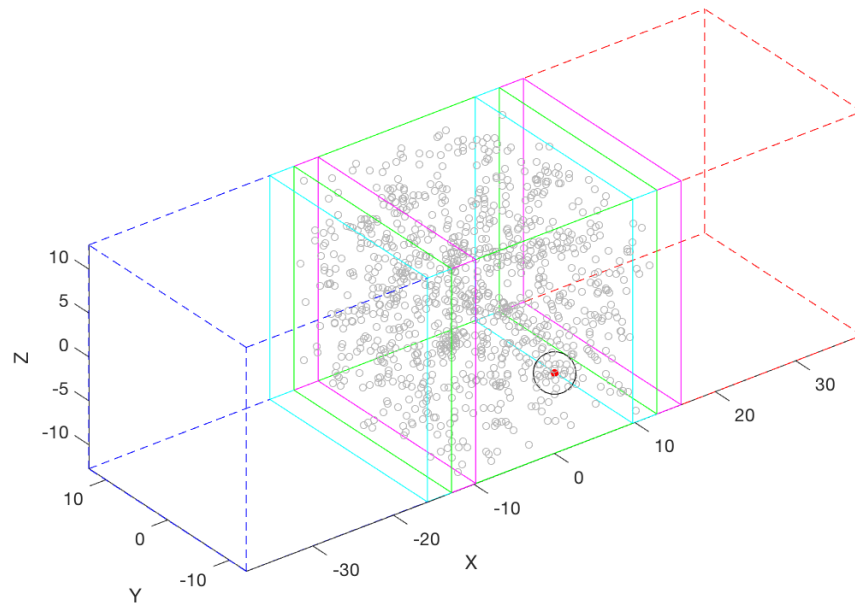


Figure 4.33. State of Particles at 5 Times of the Reference Velocity of Flow

In conclusion, the results imply that increasing the uniform flow velocity, particles tend to get closer to each other.

4.4. Time-Step Dependence of Simulations

As explained in Section 2.3.5, particles are restricted to move 5% of their diameter at a reference velocity because strong repulsive interactions yield larger errors even in one time-step. In order to see the effect of the time-step, the same system in compartment-1 of the thermal diffusion simulation, which has 1000 Argon particles at 300 Kelvin, is introduced. Average velocities of simulations 7 test cases are investigated with time-steps corresponding to 2%, 4%, 5%, 6.5%, 8%, 10% and 20% particle movement restriction, keeping the simulation duration the same as 1000 picoseconds. The results for these data points presented in Figure 4.34 show that the selected time-step is reasonable.

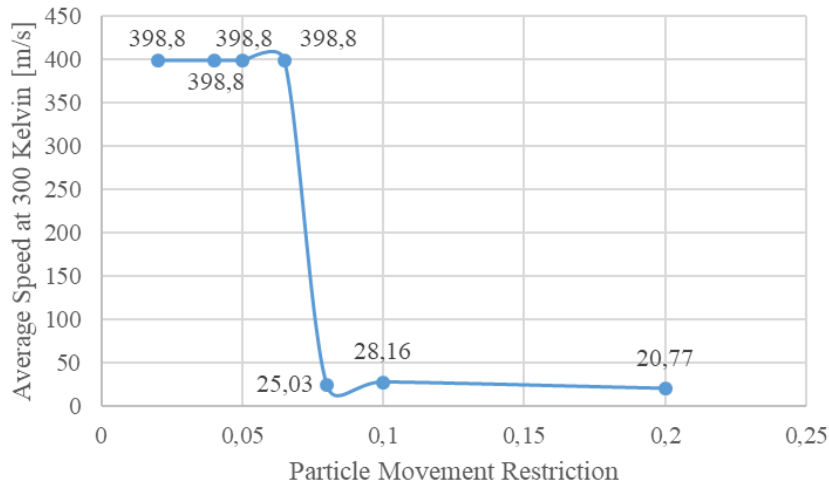


Figure 4.34. Average Velocities for Different Time-Step Selections

4.5. Time Efficiency of Simulations

Making some trial simulation runs, the average duration for one simulation time-step is observed to be dependent to the total number of particles if simulations are performed in the same computer. The average duration for one simulation time-step does not change with the time-step selection or initial average kinetic energy of particles. As it can be seen in Figure 4.35, the average durations for one simulation time-step are found as 0.001, 0.015 and 0.77 seconds for systems having 125, 1000 and 8000 particles respectively. Simulations are performed by MATLAB R2018a which is installed in a computer having Intel Core i5-5350U processor with 1.80 gigahertz base frequency and 2.90 gigahertz maximum turbo frequency.

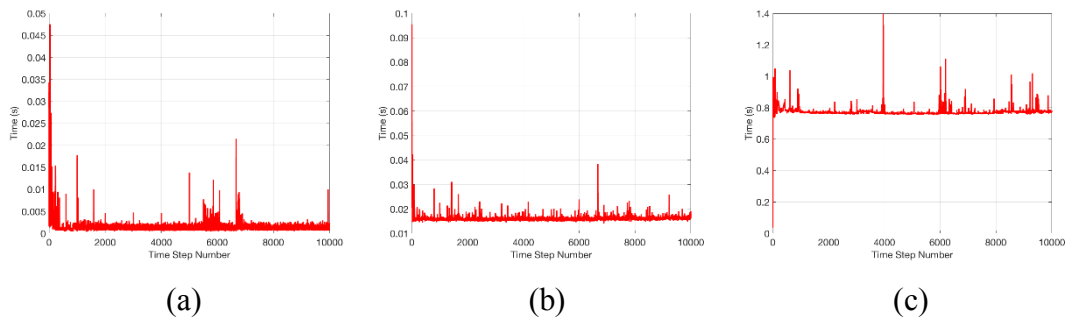


Figure 4.35. Simulation Step Durations for (a)125 (b)1000 (c)8000 Particles

The dependence of the simulation step duration to the number of system particles is presented in logarithmic scale in Figure 4.36.

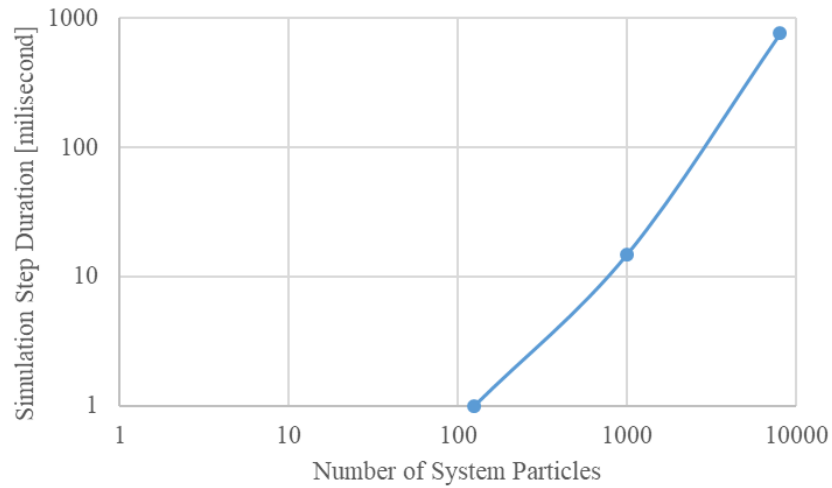


Figure 4.36. Dependence of Simulation Step Duration and Number of Particles

Durations for each simulation time-step for the thermal diffusion simulation, described in Section 4.2, are presented in Figure 4.37. Note that, in the first phase there are two separated 1000-particle systems and the average duration for one simulation time-step is 0.035 seconds. In the second phase, there is only one 2000-particle system and the average duration for one simulation time-step is 0.080 seconds.

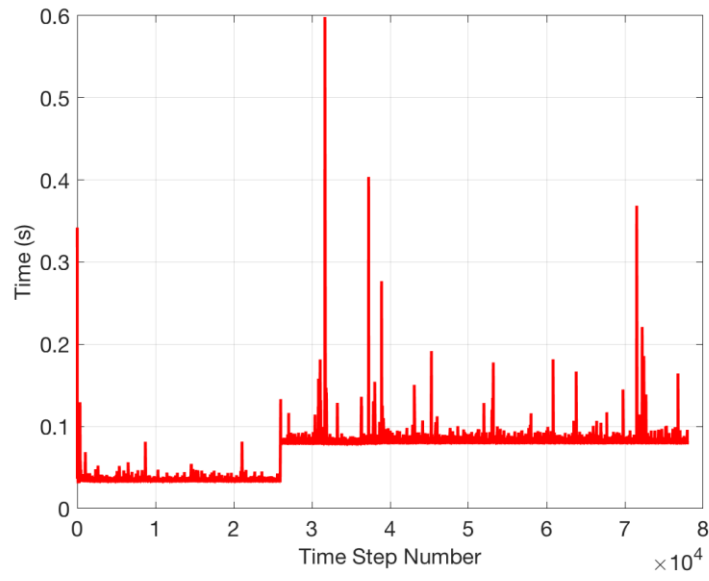


Figure 4.37. Simulation Step Durations for the Thermal Diffusion Simulation

CHAPTER 5

CONCLUSIONS

This thesis attempts to increase the accuracy of a calculation technique related to an approach proposed by Çıray [1] and implement the improved technique to thermal diffusion and unidirectional fluid flow applications. Motions of particles are taken into consideration for estimating the next potential between interacting particles for this purpose. Furthermore, the approach is converted into a simulation program, prepared in MATLAB environment. The program is structured as a main code and subroutines in order to ease the implementation for further applications.

Notable increase in accuracy is obtained as a result of the improvement in the calculation technique in the probability density function of speed distribution, the distribution of velocity vector components and the pressure results of the simulation according to corresponding results obtained during validation studies [2].

Simulation results on the thermal conductivity constant in thermal diffusion application compromise with the physical data. Furthermore, establishment of the new thermal equilibrium state between particle groups and uniform distribution of heat in the system volume are observed. In addition, the unidirectional flow simulations results indicate that increase of the uniform flow velocity results a tendency for particles to get closer to each other.

Future work of this thesis is to increase the number of particles and enlarge the simulation duration in order to seek for drawing information about understanding and structure of particle activity under turbulent flow conditions. Implementation of parallel computing techniques may be essential for this purpose. In order to further enhance the speed of the simulations, cluster methods can be applied. In addition, the accuracy of results and simulation speed can be compared with available open source

and commercial software by introducing the same problem. Furthermore, some analyses can be carried out for particle activity between unlike molecules in order to seek for exploring new concepts. Moreover, the approach can be implemented to solid mechanics' applications, such as friction and fracture phenomena, to see the performance of the approach apart from fluid mechanics. What is more, the unidirectional fluid flow simulations can be driven on investigating the formation of particle groups seeking whether there is a common behavior of particles in the groups at any time.

REFERENCES

- [1] Çıray, C. (2015). A Formulation for the Activity of Simple Molecules Part I. *8th Ankara International Aerospace Conference*, (Ankara).
- [2] Eneren, Ş. P. (2016). Validation of a Particle Simulation Approach, Middle East Technical University Graduate School of Natural and Applied Sciences, Ankara.
- [3] Karplus, M. (2002). Molecular dynamics simulations of biomolecules. *Accounts of Chemical Research*, 35(6), 321–323.
- [4] Nilsson, L., Clore, G. M., Gronenborn, A. M., Brünger, A. T., & Karplus, M. (1986). Structure refinement of oligonucleotides by molecular dynamics with nuclear overhauser effect interproton distance restraints: Application to 5' d(C-G-T-A-C-G)₂. *Journal of Molecular Biology*, 188(3), 455–475.
- [5] Marrink, S. J., Tieleman, D. P., & Mark, A. E. (2000). Molecular Dynamics Simulation of the Kinetics of Spontaneous Micelle Formation. *The Journal of Physical Chemistry B*, 104(51), 12165–12173.
- [6] Hess, B. (2002). Determining the shear viscosity of model liquids from molecular dynamics simulations. *Journal of Chemical Physics*, 116(1), 209–217.
- [7] Haughney, M., Ferrario, M., & McDonald, I. R. (1987). Molecular-dynamics simulation of liquid methanol. *Journal of Physical Chemistry*, 91(19), 4934–4940.
- [8] Rapaport, D. C., & Clementi, E. (1986). Eddy formation in obstructed fluid flow: A molecular-dynamics study. *Physical Review Letters*, 57(6), 695–698.
- [9] Korlie, M. S. (2007). 3D simulation of cracks and fractures in a molecular solid under stress and compression. *Computers and Mathematics with Applications*, 54(5), 638–650.
- [10] Yang, C., Tartaglino, U., & Persson, B. N. J. (2006). A multiscale molecular dynamics approach to contact mechanics. *European Physical Journal E*, 19(1), 47–58.
- [11] El Mahallawi, I., Abdel-Karim, R., & Naguib, A. (2001). Evaluating effect of chromium on wear performance of high manganese steels. *Materials Science and Technology*, 17(11), 1385–1390.
- [12] Fang, T. H., Wu, C. Da, & Chang, W. J. (2007). Molecular dynamics analysis of nanoimprinted Cu-Ni alloys. *Applied Surface Science*, 253(16), 6963–6968.

- [13] Zhu, R., Pan, E., & Roy, A. K. (2007). Molecular dynamics study of the stress-strain behavior of carbon-nanotube reinforced Epon 862 composites. *Materials Science and Engineering A*, 447(1–2), 51–57.
- [14] Jones, J. E. (1924). On the Determination of Molecular Fields. — II. From the Equation of State of a Gas. *Proceedings of The Royal Society A Mathematical Physical and Engineering Sciences*, 106, 463–477.
- [15] Buckingham, R.A. (1938). The classical equation of state of gaseous helium, neon and argon. *Proceedings of the Royal Society of London. Series A. Mathematical and Physical Sciences*, 168(933), 264–283.
- [16] Morse, P. M. (1929). Diatomic molecules according to the wave mechanics. II. vibrational levels. *Physical Review*, 34(1), 57–64.
- [17] Lorentz, H. A. (1881). Ueber die Anwendung des Satzes vom Virial in der kinetischen Theorie der Gase. *Annalen Der Physik*, 248(1), 127–136.
- [18] Berthelot, D. (1898). Sur le Mélange des Gaz. *Comptes Rendus de l'Académie Des Sciences*, 126, 1703–1706.
- [19] Hudson, G. H., & McCoubrey, J. (1959). Intermolecular Forces Between Unlike. *Trans. Faraday Soc.*, 56(2), 761–766.
- [20] Sikora, P. T. (1970). Combining rules for spherically symmetric intermolecular potentials. *Journal of Physics B: Atomic and Molecular Physics*, 3(11), 1475–1482.
- [21] Waldman, M., & Hagler, A. T. (1993). New combining rules for rare gas van der waals parameters. *Journal of Computational Chemistry*, 14(9), 1077–1084.
- [22] Tang, K. T., & Toennies, J. P. (1986). New combining rules for well parameters and shapes of the van der Waals potential of mixed rare gas systems. *Zeitschrift Für Physik D Atoms, Molecules and Clusters*, 1, 91–101.
- [23] Kong, C. L., & Chakrabarty, M. R. (1973). Combining rules for intermolecular potential parameters. III. Application to the exp 6 potential. *Journal of Physical Chemistry*, 77(22), 2668–2670.
- [24] Verlet, L. (1967). Computer Experiments on Classical Fluids. I. Thermodynamical Properties of Lennard-Jones Molecules. *Physical Review*, 159(1), 98–103.
- [25] Beeman, D. (1976). Some multistep methods for use in molecular dynamics calculations. *Journal of Computational Physics*, 20(2), 130–139.
- [26] Amini, M., Eastwood, J.W., Hockney, R. W. (1987). Time integration in particle models. *Computer Physics Communications*, 44(1–2), 83–93.

- [27] Heermann, D. (1990). *Computer Simulation Methods in Theoretical Physics* (2nd ed.). Berlin: Springer-Verlag.

